eLife

Reviewed Preprint
v1 • January 16, 2025
Not revised

Reviewed Preprint
v2 • February 26, 2026
Revised by authors

Reviewed Preprint
v3 • April 10, 2026
Revised by authors

For correspondence:
dujuan9981@cau.edu.cn

# These authors contribute equally to this work.

Competing interests: No competing interests declared

Funding: See page 28

Reviewing editor: Jiwon Shim, Seoul National University, Republic of Korea

Mettl5 coordinates protein production and degradation of PERIOD to regulate sleep in *Drosophila*

Xiaoyu Wu[1,#], Xingzhuo Yang[1,#], Tiantian Fu[1,#], Yikang S Rong[2], Juan Du[1]

[1]State Key Laboratory of Agricultural and Forestry Biosecurity, MOA Key Lab of Pest Monitoring and Green Management, Department of entomology, College of Plant Protection, China Agricultural University, Beijing, China • [2]MOE Key Lab of Rare Pediatric Diseases, Hengyang College of Medicine, University of South China, Hengyang, China

eLife Assessment

The authors present **useful** findings demonstrating that the RNA modification enzyme Mettl5 regulates sleep in Drosophila. Through transcriptome- and proteome-wide analyses, the authors identified downstream targets affected in heterozygous mutants and proposed that Mettl5 regulates the translation and degradation of clock genes to maintain normal sleep function. Through additional analyses, the authors provided **solid** evidence supporting this model.

https://doi.org/10.7554/eLife.103427.3.sa3

Abstract

Sleep plays a critical role in animal physiology, primarily governed by the brain, and its disruption is prevalent in various brain disorders. Mettl5 is associated with intellectual disability (ID), which often includes sleep disturbances. However, the mechanism underlying these sleep disruptions in ID remains poorly understood. In this study, we investigated the sleep phenotypes resulting from *Drosophila Mettl5* mutations. Rescue experiments revealed that *Mettl5* functions predominantly within neurons and glia marked by *Mettl5*-Gal4 to regulate sleep. Previous work established that Mettl5 forms a complex with Trmt112 to influence rRNA methylation. Notably, a mutation in *Trmt112* mutation recapitulated these sleep disturbances, implicating translational regulation by the Mettl5/Trmt112 complex. Subsequent RNA-seq and Ribo-seq analyses of $Mettl5^{1bp}$ mutants uncovered downstream effects, including altered expression of proteasome components and clock genes. Rescue experiments confirmed that the net increase in PERIOD protein underlies the sleep phenotype. This study illuminates the interplay between ribosome function, clock genes, and the proteasome in sleep regulation, highlighting the integrated roles of protein synthesis and degradation. These findings could potentially provide an example for *in vivo* study of rRNA methylation function, expand our understanding of protein homeostasis in sleep and offer insights into the sleep phenotypes associated with ID.

Introduction

Sleep is essential for animal physiology, and understanding its molecular mechanisms has significant implications for both basic research and clinical applications. Although previous studies have identified key sleep regulators (Du et al., 2021), fundamental questions remain regarding the roles of cellular processes such as protein synthesis and degradation in sleep regulation.

Growing evidence suggests a dynamic interplay between sleep regulation and protein homeostasis. Protein synthesis is particularly active during sleep (Lyons et al., 2023), while Sleep deprivation affects translational initiation (Costa et al., 2019). The proteasome, a critical mediator of ubiquitin-dependent protein degradation, regulates synapse homeostasis by

modulating ribosomal components (Costa et al., 2019), thereby influencing synaptic function. Intriguingly, proteasome components exhibit oscillating expression pattern at the transcriptional level in human cells (Desvergne et al., 2016). A recent study in *Drosophila* showed that mutation in a proteasome component alters sleep patterns (Fernández et al., 2020). Despite these advances, the precise mechanisms by which protein synthesis and degradation influence sleep, and how these processes interact, remain unresolved.

While several factors influencing proteasome assembly and subunit transcription have been identified (Kapetanou et al., 2022), the translational control of proteasome subunits remains poorly understood. Additionally, proteasome inhibition has been shown to alter ribosome function (Galimberti et al., 2016; Costa et al., 2019; Palanca et al., 2014), raising the question of whether the proteasome itself is regulated by the status of the translation machinery. Exploring this relationship could provide key insights into the interplay between proteasome activity and translation.

In *Drosophila, Mettl5* exhibits 18S ribosomal RNA m^6A methyltransferase activity (Leismann et al., 2020) and interacts with Trmt112 to facilitate this function, a mechanism conserved in human (Leismann et al., 2020; van Tran et al., 2019). Although *Mettl5* depletion abolishes m^6A modification on 18S rRNA without impairing rRNA maturation, it affects fly orientation behavior. In mammalian cells, *Mettl5*-mediated 18S rRNA N6-methyladenosine (m^6A) modification regulates stem cell fate determination and neural function (Wang et al., 2020). However, it remains unclear whether *Mettl5* modulates global or transcript-specific translation profile *in vivo*, particularly in tissues rather than cell lines. Moreover, while *Mettl5* is linked to intellectual disability (ID) with comorbid sleep disturbances, its mechanistic role in these disorders is unknown. Testing whether *Mettl5* loss affects behaviors like sleep in *Drosophila* could clarify this connection.

We discovered that *Mettl5* regulates sleep in *Drosophila*. To investigate the underlying mechanism, we performed RNA-seq and Ribo-seq on *Mettl5* mutants, revealing dysregulation of multiple clock genes and proteasome components. This suggests *Mettl5* coordinates protein production and degradation, which are crucial for protein homeostasis. Follow-up experiments confirmed that the protein level of Period was upregulated in *Mettl5* mutants, contributing to the sleep phenotype. This study highlights that ribosome defects can perturb proteasome function, uncovering a mechanism that couples protein degradation with synthesis. Additionally, by mapping the genome-wide downstream gene profile of an rRNA methylation modifier, this study offers insights into the gene-specific roles of ribosome function.

Results

Mettl5 regulates sleep in *Drosophila*

Mettl5 contains a predicted N6 adenine specific nucleic acids methyltransferase domain. In order to study the function of this gene in sleep regulation, we generated CRISPR-Cas9 knockout mutants. We created two alleles. $Mettl5^{1bp}$, which deleted 1bp in the coding region results in a truncated version (Figure 1A) and down regulation of *Mettl5* at mRNA level (Figure 1B). Another allele $Mettl5^{9bp}$, which results in 3 amino acids deleted version of *Mettl5* (Figure 1A) does not cause significant change at mRNA level (Figure 1B). We found that heterozygous $Mettl5^{1bp}$ mutants exhibited significantly reduced nighttime sleep (Figure 1C-G), particularly during early night (ZT12-ZT16; Figure 1C). Quantitative analysis revealed increased wakefulness at ZT14 in mutants (Figure 1H). 'awake %' was used to indicate the percentage of awake fruit fly population at specific time points (e.g., ZT14). quantitative nighttime sleep latency measurements indicated a delayed sleep start in mutants (Figure S1G). In addition, *Mettl5* expression was significantly up regulated during the sleep recovery period after mechanical sleep deprivation (Figure 1I-J). *Mettl5* mutant displayed significantly increased sleep rebound in 24 hours after sleep deprivation (Figure 1K-L), indicating its effects on sleep homeostasis. Moreover, results of

sleep arousal assay at ZT19 indicated that the percentage of aroused flies are significantly more than the control group (Figure 1M). These results demonstrate that the truncated *Mettl5* mutation causes sleep deficits, establishing *Mettl5* as a novel sleep regulator in *Drosophila*.

To confirm the specificity of the sleep phenotype in $Mettl5^{1bp}$, we performed genetic rescue experiments. Introduction of a single wild-type *Mettl5* copy completely rescued both the reduced sleep amount and increased wakefulness at ZT14 (Figure 1N-R), demonstrating that these phenotypes specifically result from *Mettl5* deficiency.

The observed expression pattern of *Mettl5* further supports its sleep regulatory function. Using *Mettl5*-Gal4 reporter lines, we found expression in both neurons (colocalizing with ELAV staining; Figure S1A-C) and glial cells (colocalizing with Repo staining; Figure S1D-F). Behavioral analyses revealed additional mutant phenotypes consistent with sleep dysregulation. we tested the climbing ability of *Mettl5* mutation which showed an increase (Figure S1H). RNAi knocking down of *Mettl5* showed a consistent phenotype of down regulated sleep amount during the night time (Figure S1I-L).

Mettl5 regulates *Drosophila* sleep through its methyltransferase activity

Previous studies established that Mettl5 interacts with Trmt112 to regulate 18S rRNA m^6A modification (Leismann et al., 2020; van Tran et al., 2019). Consistent with these findings, our LC-MS/MS analysis revealed significantly reduced m^6A levels in both total RNA and 18S rRNA from heterozygous $Mettl5^{1bp}$ (Figure 2A-B). To determine whether Mettl5's sleep regulatory function depends on its methyltransferase activity, we performed two key experiments. First, we examined the phenotype of *Trmt112* knockdown. We found that the *Mettl5*-Gal4 driven *Trmt112* RNAi resulted in a similar phenotype to $Mettl5^{1bp}$ (Figure 2C-G), suggesting that *Mettl5* regulates sleep through its 18S rRNA m^6A modification activity. The efficiency of the *Trmt112* RNAi line was tested in previous study (López-Varea et al., 2021). More important, we performed a rescue experiment with a mutated form of *Mettl5* that lacks the NPPF amino acids required for its methyltransferase activity (Figure2A) (Iyer et al., 2016). We observed that this mutant *Mettl5* failed to rescue the sleep phenotype caused by $Mettl5^{1bp}$ (Figure 2H-L). Together, these results demonstrate that Mettl5's methyltransferase activity is essential for its role in sleep regulation, likely through its function in 18S rRNA m^6A modification.

RNA-seq and Ribo-seq revealed the downstream gene profile of *Mettl5*

To better understand the downstream events of *Mettl5*, we performed RNA-seq and Ribo-seq to assess transcriptomic and translational changes in $Mettl5^{1bp}$. Principal Coordinates Analysis (PCoA) of RNA-seq and Ribo-seq datasets revealed clear separation between mutant and control groups (Figure S2A, B, D, E). High reproducibility was found among biological replicates (Figure S2C, F), confirming data quality. Transcriptome analysis identified 1,053 significantly differentially expressed genes ($|\log_2(\text{Fold Change})| \geq 1$ & $p^{adj} < 0.05$), comprising 217 upregulated and 836 downregulated transcripts (Figure 3A, B). Parallel ribosome profiling revealed 299 translationally regulated genes ($|\log_2(\text{Fold Change})| \geq 0.265$ & $p^{adj} < 0.05$), with 149 upregulated and 150 downregulated targets compared to the controls (Figure 3C). Heatmaps of the top 100 differentially expressed genes from both RNA-seq and Ribo-seq analyses were generated according to the rlog transformed values (Figure S3A, B).

To explore the biological implication of differentially expressed genes at transcriptional and translational levels, we performed Gene Ontology (GO) enrichment analysis. At the transcriptional level (Figure S4A, C), the most significantly enriched biological processes included cellular response to chemical stimulus, small molecule biosynthetic process, and fatty acid metabolic process (Figure S4A), with supporting gene networks (Figure S4C). Translational-level analysis (Figure S4B, D) revealed prominent enrichment for organic acid and amino acid metabolic

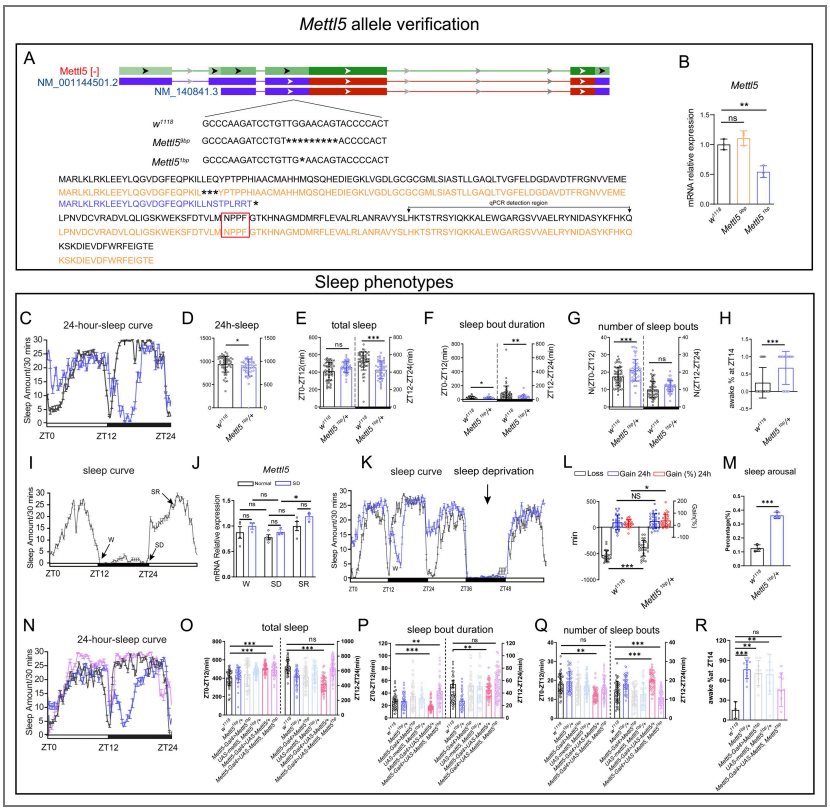

Figure 1. **Mettl5 is a regulator of *Drosophila* sleep.**

(A) Diagram illustrating CRISPR-Cas knockout of 1 or 9 bases in the *Mettl5* gene. The corresponding protein sequence is listed with the predicted N6 adenine specific nucleic acids methyltransferase domain highlighted in the red box. (B) Relative expression of *Mettl5* mRNA in homozygous *Mettl5*^{1bp} and *Mettl5*^{9bp}mutant male flies compared to control flies. (C) Sleep curve throughout the day for *Mettl5* mutant male flies (blue) and control flies (black). (D) Total sleep of *Mettl5* mutant male flies and control flies in 24 hours. (E) Total sleep of *Mettl5* mutant male flies and control flies within day and night, respectively. (F) Sleep bout duration of *Mettl5* mutant male flies and control flies. (G) Number of sleep bouts of *Mettl5* mutant male flies and control flies. (H) Percentage of awake for *Mettl5* mutant flies and control flies. (I) Sleep curve is tracked throughout the entire day prior to sleep deprivation and during the daytime sleep rebound period. (J) *Mettl5* mRNA expression level at different time points. W(wake), SD (sleep deprivation), SR (sleep recovery). (K) Sleep curve is tracked throughout the entire day prior to sleep deprivation and during the daytime sleep rebound period in *Mettl5* mutant male flies (blue) and control flies (black). (L) Response to sleep deprivation and performance measures in *Mettl5* mutants and controls. Black bars represent the amount of sleep lost during the 24-hour sleep deprivation period, blue bars indicate the amount of sleep regained, whereas the red bars indicate the proportion of sleep recovered (right y-axis). (M) Sleep arousal of *Mettl5*^{1bp} male flies and control flies at ZT19. (N) Sleep curve throughout the day for the following genotypes: *w*^{1118}(black), *Mettl5*^{1bp}/+ (blue), *and Mettl5-Gal4, UAS-Mettl5, Mettl5*^{1bp}/+(pink). (O) Total sleep of the indicated genotypes. (P) Sleep bout duration of the indicated genotypes. (Q) Number of sleep bouts of the indicated genotypes. (R) Percentage of awake for the indicated genotypes. For * stands for p<0.05, ** stands for p<0.01, *** stands for p<0.001, *ns* stands for not significant. For letter-based annotations, Groups with no significant differences share the same letter, Groups with significant differences are assigned new letters.

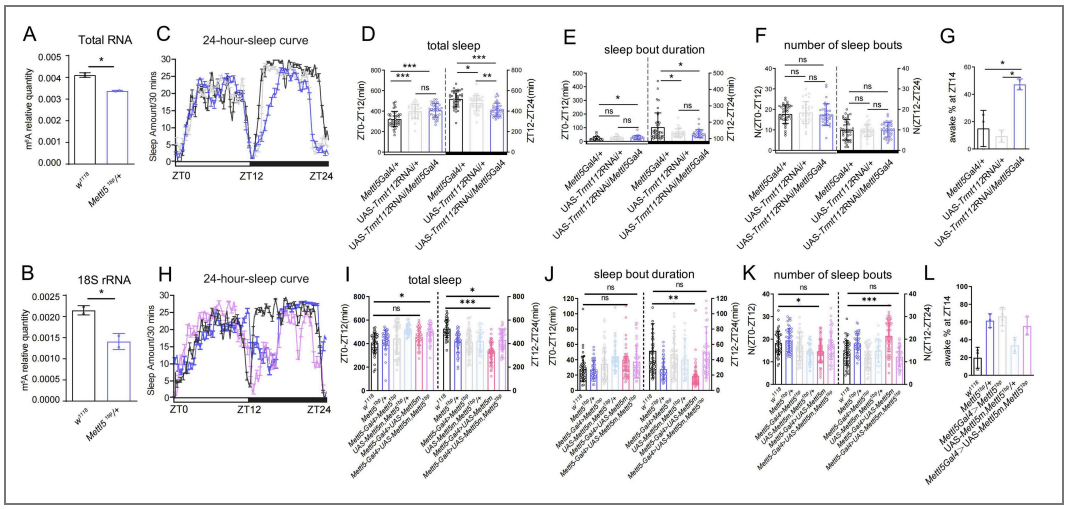

Figure 2. Mettl5 regulation of *Drosophila* sleep was dependent on its methyltransferase activity.

(A) The m^{6}A level in the total RNA of *Mettl5* mutant male flies. (B) The m^{6}A level in the 18S rRNA of *Mettl5* mutant male flies. (C) The sleep curve throughout the day shows the sleep pattern of induced *Trmt112* RNAi male flies and control flies. (D) Total sleep of induced *Trmt112* RNAi male flies and control flies. (E) Sleep bout duration in induced *Trmt112* RNAi male flies and control flies. (F) Number of sleep bouts in induced *Trmt112* RNAi male flies and control flies. (G) Percentage of awake in *Trmt112* RNAi and control flies. (H) Sleep curve throughout the day for *Mettl5* mutant male flies, induced *Mettl5m* over expression male flies and control flies. (I) Total sleep of *Mettl5* mutant male flies, induced *Mettl5m* over expression male flies and control flies. (J) Sleep bout duration in *Mettl5* mutant male flies, induced *Mettl5* over expression male flies and control flies. (K) Number of sleep bouts in *Mettl5* mutant male flies, induced *Mettl5* over expression male flies and control flies. (L) Percentage of awake in *Mettl5* mutant male flies, induced *Mettl5* over expression male flies and control flies. For * stands for p<0.05, ** stands for p<0.01, *** stands for p<0.001, *ns* stands for not significant. For letter-based annotations, Groups with no significant differences share the same letter, Groups with significant differences are assigned new letters.

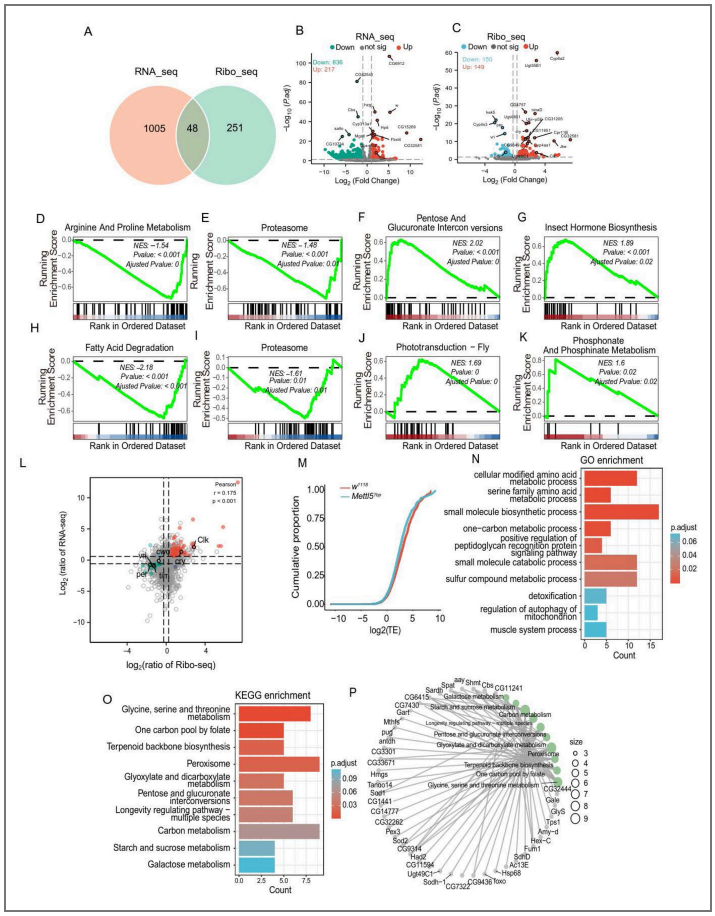

Figure 3. RNA-seq and Ribo-seq analysis revealed changes in the gene profile of *Mettl5*^{1bp}.

(A) Venn diagram depicting the number of significant differentially expressed genes revealed by RNA-seq and Ribo-seq. (B) Volcano plot representing the differentially expressed genes identified by RNA-seq. Genes that met the criteria of |log2(fold-change)| ≥ 1 and p.adjust < 0.05 were considered significantly expressed, marked in orange for downregulation and green for upregulation, comparing with the controls. (C) Volcano plot representing the differentially expressed genes identified by Ribo-seq. Candidates that satisfied the criteria of $|\log_2(\text{fold-change})| \geq 0.265$ and p.adjust <0.05 were regarded as significantly expressed, marked in red for downregulation and blue for upregulation, respectively. (D-K) Gene set enrichment analysis of differentially expressed genes revealed by RNA-seq (D-G) and Ribo-seq (H-K). All the plots are generated using the KEGG gene set database. The bar chart at the bottom of each panel shows the distribution of target genes for each pathway according to their rank position. Each vertical line represents a gene. Genes on the left show positive correlation with *Mettl5*^{1bp}, while, genes on the right show negative correlation with *Mettl5*^{1bp}. The green line indicates the enrichment score (ES), and NES stands for normalized enrichment score. (L) Distribution of the differentially expressed genes revealed by both RNA-seq and Ribo-seq. (M) Cumulative distribution of TE frequencies among w^{1118} and *Mettl5*^{1bp} (N, O) GO and KEGG enrichment of significantly changed TE-related genes between $w^{1118}$and *Mettl5*^{1bp}. The color of the bar indicates the enrichment p.adjust value. (P) KEGG network showing the top 10 pathway and associated genes. The size of the dots represents the number of genes in the pathway.

processes, lipid catabolism, cellular respiration, and transport mechanisms. Notably, we identified strong associations with circadian regulation, including circadian regulation of gene expression and entrainment of the circadian clock.

The GO results usually contain a long list of enriched terms that have highly redundant information and are difficult to summarize. So, we performed a simplify Enrichment analysis that visualizes the summaries of clusters by word cloud for the GO enrichment result at transcriptional and translational levels. For transcriptionally significant DEGs (Figure S5A), major enriched processes included metabolic and stimulus-response pathways, wing disc and imaginal system development, ion-channel homeostasis and transport, and cytokinesis/cell cycle transitions. Translationally regulated genes additionally showed enrichment for sleep-wake cycles, circadian behavior, and neuronal cell death (Figure S5D). Cellular component analysis highlighted chromosomal structures, membrane-bound complexes, and vesicles (Figure S5B), while molecular functions predominantly involved enzymatic activities, ion/protein binding, receptor activities, and transcription processes (Figure S5C). The strong concordance between RNA-seq and Ribo-seq enrichment profiles (Figure S5E-F) further validated these findings.

Our Gene Set Enrichment Analysis (GSEA) identified pathways enriched in differentially expressed genes at both transcriptional and translational levels. To capture subtle but biologically important changes that might be excluded by stringent statistical thresholds, we analyzed gene sets ranked by log2 fold-change without p-value filtering. The GSEA-GO and GSEA-KEGG results, sorted by Normalized Enrichment Score (NES), revealed several key pathways (Figure S6A-D). Notably, the proteasome pathway showed significant suppression at both transcriptional and translational levels (P.adjust<0.05) (Figure 3E, I). Transcriptional-level analysis highlighted disruptions in arginine and proline metabolism and insect hormone biosynthesis (P.adjust<0.05) (Figure 3D, G). While, while translational changes predominantly affected fatty acid degradation and phosphonate/phosphinate metabolism (P.adjust<0.05) (Figure 3H-K).

To better understand the correlation between transcription and translation levels, we performed correlation analysis of differentially expressed genes based on fold change of DEGs (Figure 3L). 977 genes showed opposing trends between transcription and translation, while only 24 genes exhibited concordant changes. We identified 240 translation-specific and 3,309 transcription-specific DEGs, with each cluster undergoing separate enrichment analysis (Figure S7A-H). Notably, core clock genes (*Clk*, *tim*, etc.) displayed significant changes at both levels (Figure 3L).

To isolate translational effects, we calculated translation efficiency (TE) differences between $Mettl5^{1bp}$ and w^{1118}controls (Figure 3M). Among 1,204 genes with significantly altered TE, GO enrichment highlighted amino acid metabolism and small molecule biosynthesis (Figure 3N), while KEGG analysis emphasized glycine/serine/threonine metabolism and one-carbon pool by folate pathways (Figure 3O, P).

Ribo-seq revealed the $Mettl5^{1bp}$ led to changes of some global translation features

Using Ribo-seq, we compared global translation features between the w^{1118} and $Mettl5^{1b}$ groups. The TE (translation efficiency) correlation coefficients among the three biological replicates of each genotype ranged from 0.87 to 0.93, demonstrating high reproducibility within genotypes (Figure S8A-F). We found that the length of ribosome-protected RNA fragments (RPFs) was approximately 28nt (Figure S10A). The RPFs exhibited a significant 3-nt periodicity. Metagene analysis of individual 28nt reads revealed the distribution of RPFs across the gene locus in w^{1118} and $Mettl5^{1bp}$, respectively (Figure S8, S9). The starting point of translation is 12nt upstream of start-codon and gradually disappears 15nt from stop-codon (Figure S8G-L). RPFs on the metagene plot distribution around the translation start and translation stop site (Figure S9A-F), different coding frames on CDS, 3'-UTR and 5'-UTR, respectively in two groups of samples all showed the periodicity (Figure S9G-L). As expected, all plots show an enrichment of P-sites in the first frame on the coding sequence but not the UTRs, in accord with ribosome protected fragments from protein coding mRNAs (Figure S9G-L).

Analysis of open reading frame (ORF) types revealed alterations in their distribution. Compared to w^{1118}, $Mettl5^{1bp}$ exhibited an increased proportion of overlapping downstream ORFs (dORFs) and fewer non-overlapping dORFs (Figure S10B). In both groups, translated upstream ORFs (uORFs) were significantly shorter than untranslated uORFs ($P < 0.05$) (Figure S10C). Additionally, $Mettl5^{1bp}$ displayed reduced read counts for both dORFs and uORFs (Figure S10D-E). Based on translation potential, uORFs were classified as either translated or untranslated, and motif analysis was performed separately for each category (Figure S10F-G).

Mutation of *Mettl5* altered codon preference

Comparison of codon occupancy (A-site) between the two groups revealed that *Mettl51bp* preferentially used GAC and GAU, whereas *w1118* favored UCC (Figure S10H). This trend was further supported by the cumulative frequency distribution of these codons (Figure S10I-K). Since GAC and GAU both encode aspartate (Asp), we analyzed Asp amino acid occupancy. Intriguingly, Asp was significantly enriched in *w1118* during translation (Figure S10L), suggesting that *Mettl51bp* may exhibit altered translational regulation (see Discussion for details).

Metagene analysis of RPFs revealed distinct translation patterns between $Mettl5^{1bp}$ and w^{1118}. The coding sequence (CDS) and flanking regions were segmented into 100 equal bins, and average RPF density was computed for each bin. The resulting plots illustrate differences in ribosome occupancy between $Mettl5^{1bp}$ and w^{1118} along the CDS (Figure S10M), near the translation start site (Figure S10N) and around the translation termination site (Figure S10O). Notably, $Mettl5^{1bp}$ and w^{1118} exhibited divergent ribosome occupancy patterns, particularly along the CDS and near the start codon (Figure S10M, N), suggesting potential differences in translation dynamics and initiation efficiency.

Mettl5 regulates the clock gene regulatory loop

Our findings demonstrate that *Mettl51bp* disrupts the core clock gene regulatory loop controlling circadian rhythm. We observed significant alterations in both transcriptional and translational levels of multiple clock genes, with *Cry* and *Clock* showing upregulation while *Tim, per, vri*, and *pdp1* were downregulated at both levels (Figure 4A-B). Notably, *per, vri*, and *pdp1* exhibited particularly pronounced downregulation in translation efficiency (Figure 4C). These changes occurred without affecting clock neuron morphology at different time points (Figure S11).

The observed expression patterns revealed an unexpected regulatory relationship: while the canonical clock circuitry positions *Per* downstream of *Clock*, our finding that *Clock* was upregulated while *per* was downregulated suggests *Per* may actually function upstream of *Clock* in *Mettl5*-mediated regulation. Surprisingly, despite the transcriptional downregulation of *per* (Figure 4D), we detected increased PER protein levels through both immunostaining and western blot analyses (Figure 4E-H). Detection of the PER protein at different time points indicated that it was increased at both ZT 0 and ZT18 (Figure 4E-F). This apparent contradiction aligns with the observed circadian phenotype, as *Mettl5* mutants showed significantly longer period lengths (Table 1), mirroring effects seen when PER stabilization results from reduced kinase activity as previously reported (Philpott et al., 2023). Genetic epistasis experiments further supported this model, with clock gene mutants modified *Mettl5* mutant phenotypes that suggesting both *Clock* and *Per* downstream of *Mettl5* (Figure 4I-N, Table 1). Secondary effect may exist for the significant increase in daytime sleep in the double mutants. Together, these results indicate that $Mettl5^{1bp}$ affects circadian regulation through mechanisms that extend beyond transcriptional control, likely involving post-translational regulation of PER protein stability.

To investigate the factors mediating PER protein level changes in *Mettl5* mutants, we examined the ubiquitin-proteasome pathway, which plays a well-documented role in Period protein degradation (Grima et al., 2002; Ko et al., 2002; Chiu et al., 2008). Notably, recent evidence indicates that N6-methyladenosine (m6A) regulates the ubiquitin-proteasome system in other biological contexts (Sun et al., 2023). Our integrated analysis of RNA-seq and Ribo-seq data revealed significant downregulation of multiple proteasome pathway components in $Mettl5^{1bp}$ mutants at both transcriptional and translational levels (Figures 3E, 3I, 4O), suggesting impaired protein

Figure 4. Clock genes expression mediated the sleep phenotype caused by *Mettl5* mutation.

(A-C) Fold changes in clock genes with significant expression level differences between w^{1118} and $Mettl5^{1bp}$ were observed in RNA-seq, Ribo-seq, and translation efficiency analyses. (D) The gene expression levels of per at 4 different timepoints of w^{1118} and $Mettl5^{1bp}$. (E) Western blot analysis of PER protein and Tubulin protein at 4 different timepoints, (F) along with their ratio quantification. (G) Representative image of PER protein immunofluorescence staining at ZT0 in the small ventral lateral neurons (small LNvs). (H) Statistical analysis of the immunofluorescence intensity for PER in small LNvs. (I) Sleep curve throughout the day for $Mettl5^{1bp}$, per^{01}, double mutant and control flies. (J) Total sleep for $Mettl5^{1bp}$, per^{01}, double mutant and control flies. (K) Percentage of awake time in $Mettl5^{1bp}$ flies, partially rescued by double mutant flies. (L) Sleep curve throughout the day for $Mettl5^{1bp}$, per^{01}, double mutant and control flies. (M) Total sleep for $Mettl5^{1bp}$, per^{01}, double mutant and control flies. (N) Percentage of awake time in $Mettl5^{1bp}$ flies, partially rescued by double mutant flies. (O) Fold changes in proteasome subunits with significant expression level differences between w^{1118} and $Mettl5^{1bp}$ were observed in RNA-seq, Ribo-seq, and translation efficiency analyses. For statistical significance, * stands for p<0.05, ** stands for p<0.01, *** stands for p<0.001, *ns* stands for not significant.

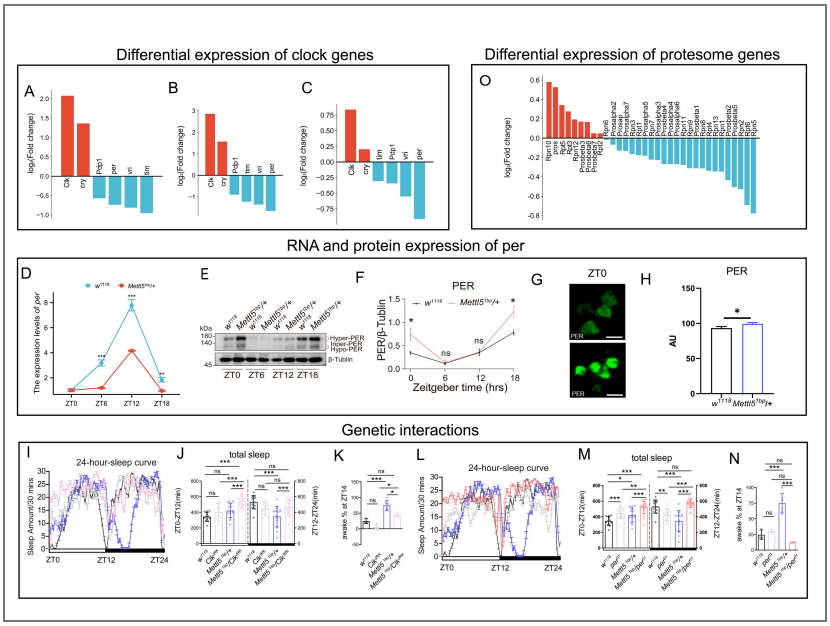

Table 1. Circadian rhythm phenotypes of various mutants.

Genotype	NumTotal	%Rhythmic	Period	Power
w^{1118}	32	92.6	23.9± 0.05	127.9± 7.62
Mettl5 ^{1bp}/+	32	92.3	28.3± 0.4 ***	114.3± 6.76 ns
Mettl5 ^{1bp}/+ ; UAS-*Mettl5*/*Mettl5*Gal4	32	96.9	24± 0.02 ns	127.1± 5.42 ns
Mettl5 ^{1bp}/*Clk*^{JRK}	44	29.5	24± 0.04 ns	68.5± 8.85 ***
Mettl5 ^{1bp}/*Per*^{01}	54	9.3	24.2± 0.2 ns	43.8± 13.41 ***

degradation capacity. Based on these findings, we propose a model where *Mettl5* regulates circadian function through three interconnected mechanisms: first, by directly modulating proteasome components to control PER protein stability post-translationally; second, by transcriptionally and translationally regulating Per and other clock expression. In this model, $Mettl5^{1bp}$-induced proteasome downregulation leads to PER accumulation, which is responsible for the phenotypes (Figure 5).

$Mettl5^{1bp}$ alters axon complexity

Previous studies have established a strong correlation between sleep homeostasis and synaptic complexity (Bushey et al., 2011). Additionally, synaptogenesis has been shown to enhance proteasome activity in axons (Costa et al., 2019). Given our observations of impaired sleep rebound following deprivation and altered expression of proteasome subunits in $Mettl5^{1bp}$ mutants, we sought to examine potential effects on synaptic complexity.

To assess synaptic complexity, we adapted an established quantification method (Bushey et al., 2011) using Syt-GFP, a marker that colocalizes with endogenous synaptic vesicles, to visualize presynaptic morphology changes. Control experiments with UAS-*Fmr1* and *Fmr1* mutations successfully replicated the expected decrease and increase in syt-eGFP signal, respectively (Figure 6A-D). Strikingly, $Mettl5^{1bp}$ mutants exhibited significantly increased syt-eGFP fluorescence in presynaptic terminals (Figure 6E-M), indicating altered synaptic complexity.

Discussion

Our study reveals that Mettl5, a known rRNA methyltransferase, modulates sleep through its RNA methylation activity. Through integrated RNA-seq and Ribo-seq analyses of $Mettl5^{1bp}$mutants, we identified *Mettl5*'s downstream targets at both transcriptional and translational levels. Further investigation demonstrated that Mettl5 influences sleep regulation by affecting two key pathways: the circadian clock gene network and the proteasome system. These findings provide novel mechanistic insights into sleep control, highlighting the coordinated role of protein synthesis and degradation in this process. Notably, our Ribo-seq analysis revealed that $Mettl5^{1bp}$ alters fundamental translation features, including uORF translation efficiency and codon preference, suggesting rRNA methylation plays a regulatory role in these processes.

This discovery has important clinical implications, as METTL5, the human ortholog of Mettl5, is associated with intellectual disability (ID) when mutated (Richard et al., 2019). Our work expands the understanding of Mettl5's molecular function and may inform potential therapeutic strategies for ID. The clinical relevance of our findings is underscored by reports of sleep disturbances, particularly reduced sleep duration, in ID patients - a phenotype that parallels our observations in $Mettl5^{1bp}$ mutants. The mechanistic framework established in this study could explain these clinical sleep abnormalities. However, further validation in vertebrate models is needed to determine whether this regulatory mechanism is evolutionarily conserved and applicable to human sleep disorders.

As shown in Table 1, the $Mettl5^{1bp}$/+ mutant exhibits a robust long-period phenotype, with circadian rhythms significantly extended to 28.3 ± 0.4 hours compared to the wild-type's 23.9 ± 0.05 hours. This prolonged period perfectly aligns with the observed behavioral phenotypes, including delayed nighttime sleep onset, later daytime waking, and the overall shift in sleep profile. This is indeed quite similar to previous report on Period3 variant (Zhang et al., 2016). We think that the prolonged circadian period contributes to the observed sleep phenotype. However, since total sleep time was significantly reduced in the mutant, we cannot attribute the phenotype solely to period lengthening. Furthermore, our 24-hour PER expression analysis in *Mettl5* mutants revealed elevated PER protein levels at ZT1 and ZT18, while ZT6 and ZT12 showed no significant changes, with no apparent phase shift. These findings collectively suggest that the phenotype primarily results from PER protein stabilization and accumulation.

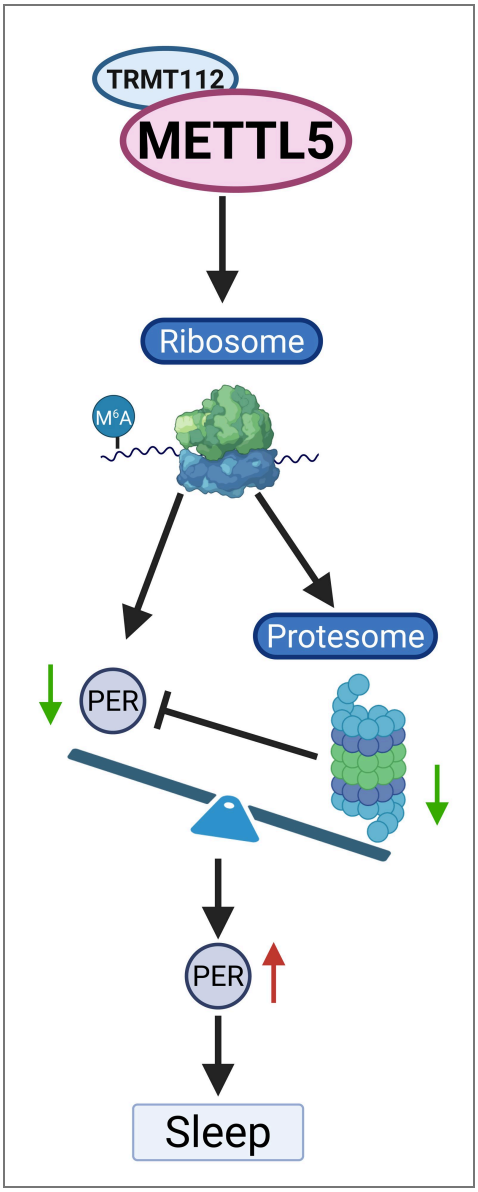

Figure 5. **A working model illustrating the role of *Mettl5* in *Drosophila* sleep was presented.**

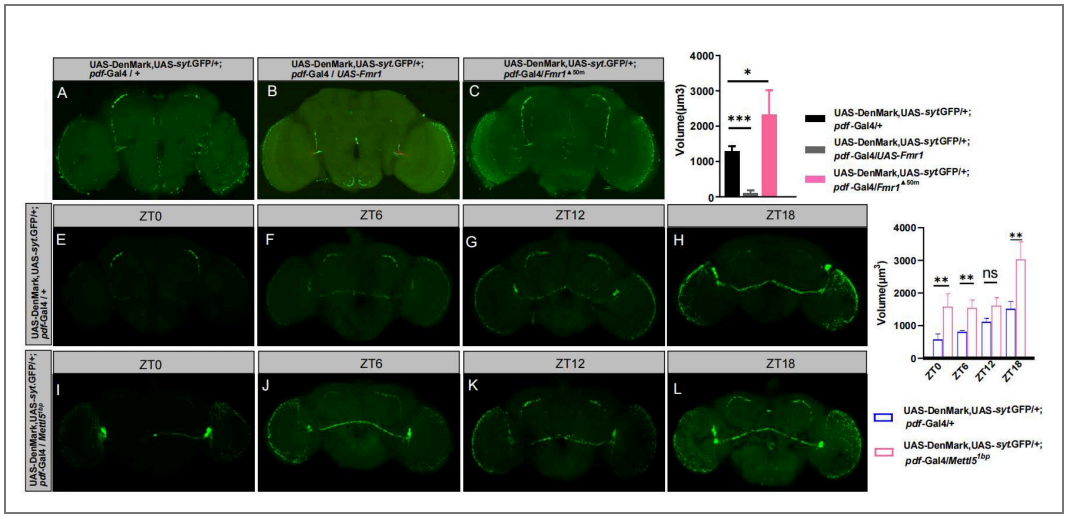

Figure 6. The axon complexity was found to be affected by *Mettl5*^{1bp}

(A–C) Representative confocal micrographs of small ventral lateral neuron (s-LNv) axonal terminals across different genotypes. Presynaptic structures were visualized using *syt*-eGFP (green), which colocalizes with endogenous synaptic vesicles: (A) control (B) Fmr1 overexpression and (C) Fmr1 null mutant. (D) Quantification of s-LNv axonal terminal volumes corresponding to genotypes in (A–C). (E–H) Representative images of axonal terminal morphology in control flies at four time points: ZT0, ZT6, ZT12, and ZT18. (I–L) Representative images of axonal terminal morphology in *Mettl5* mutant flies at ZT0, ZT6, ZT12, and ZT18. (M) Quantitative comparison of axonal terminal volumes between control and Mettl5 mutant flies at different time points. Scale bar: 50 μm. For statistical significance, * stands for p<0.05, ** stands for p<0.01, *** stands for p<0.001, *ns* stands for not significant.

We found that *Mettl5* heterozygotes showed significant reductions in total RNA and 18S rRNA methylation levels, contrasting with mouse studies where heterozygous knockouts maintained normal 18S rRNA m6A methylation (Sepich-Poore et al., 2022). This discrepancy may stem from either fundamental differences in rRNA methylation regulation between *Drosophila* and mice, or distinct biological consequences of knockdown versus knockout approaches, as complete gene elimination often triggers compensatory mechanisms (Teng et al., 2013; Rossi et al., 2015; Vu et al., 2015; Ma et al., 2019; El-Brolosy et al., 2019).

Our study uncovers a previously unrecognized connection between circadian clock genes and proteasome function. While previous work demonstrated that the circadian clock rhythmically regulates proteasome components in *Drosophila* fat bodies under dietary restriction (Hwangbo et al., 2023), we now show that *Mettl5* modulates clock protein synthesis and degradation in clock neurons by influencing proteasome activity. This regulation likely occurs through *Mettl5*-mediated ribosomal methylation in clock neurons, which impacts the proteasome degradation pathway (Costa et al., 2019), ultimately altering clock protein dynamics.

Mettl5 represents a novel integrator of rRNA methylation and proteasome function, providing a mechanism to balance protein synthesis and degradation. Interestingly, we observed specific effects on both transcriptional and translational outputs, with particular proteasome subunits showing differential regulation. This specificity may arise from either selective translational control by Mettl5 or additional layers of regulation through protein-protein interactions. These findings suggest an intricate regulatory network coordinating these processes, though further studies are needed to elucidate the underlying mechanisms.

Our results reveal complex relationships between clock genes and sleep regulation. While *cyc* loss-of-function alleles show enhanced sleep rebound in females (Shaw et al., 2002), $Mettl5^{1bp}$mutants with elevated PER protein exhibit reduced rebound. Notably, *Mettl5*'s regulatory effects display tissue specificity - although absent in canonical clock neurons, *Mettl5*-Gal4 is expressed in distinct neurons and glia that appear crucial for sleep regulation. This expression pattern, combined with Clock's broader distribution (Patop et al., 2023), suggests specialized circuits for sleep homeostasis that warrant further investigation.

Evidence indicates that sleep functions in development, metabolism and neuronal plasticity (Anafi et al., 2019). Sleep exerts effects on neuronal plasticity by modifying synapses. The synaptic homeostasis theory proposes that sleep has a role in downscale synaptic strength (Tononi and Cirelli, 2006). Indeed, synapse markers progressively decrease during sleep in both mammals and *Drosophila* brains (López-Varea et al., 2021; Vyazovskiy et al., 2008; Gilestro et al., 2009; Liu et al., 2010) More importantly, evidence indicates that sleep need and protein levels in synapse are tightly linked. Studies of the presynaptic active zone have shown that synaptic plasticity regulates sleep homeostasis (Huang et al., 2020). Genome-wide proteomic studies of synapse in mouse brain indicate that the synaptic proteins peak around dusk and dawn (Noya et al., 2019; Brüning et al., 2019). Sleep deprivation experiments have demonstrated that the sleep drive is significantly dependent on the cycling of proteins and phosphoproteins in synapses, in contrast to mRNAs (Noya et al., 2019; Brüning et al., 2019). These results suggest that the gene expression regulation at the protein level is crucial for sleep. Consistently, we detected changes in the quantity of axons in $Mettl5^{1bp}$, suggesting a possible regulation of neural circuits by *Mettl5*.

The mechanism by which METTL5 regulates translation warrants further investigation. Previous studies have demonstrated that METTL5 influences translation (Rong et al., 2020; Peng et al., 2022), but whether the mechanisms identified here are conserved across other systems remains an intriguing question. In our analysis, we observed increased usage of aspartate (Asp) codons in *Mettl5* mutants. Notably, prior work has linked codon usage to PER protein function—specifically, a codon-optimized version of PER failed to rescue circadian rhythmicity in *per* mutant flies, unlike the wild-type version (Fu et al., 2016). Further analysis revealed that PER protein levels were elevated in these mutants, suggesting that codon optimization enhances PER expression (Figure 2B in Fu et al., 2016). Strikingly, when we examined the codon-optimized region from Fu et al. (2016), we found that GAC (Asp) was highly enriched, raising the possibility that *Mettl5*

mutation affects PER protein accumulation by altering GAC codon usage. Additional experiments will be needed to validate this hypothesis. Furthermore, we detected changes in upstream open reading frames (uORFs) in *Mettl5* mutants, but their relationship to translational regulation requires further exploration.

Our study demonstrates that ribosomal components can exert gene-specific regulatory functions, building upon previous work showing context-dependent ribosome specialization (Simsek et al., 2017). In *Mettl5* mutants, we observed distinct alterations in the translational efficiency of specific genes. These effects could potentially arise through two non-exclusive mechanisms: (1) *Mettl5*-mediated rRNA modifications may modulate ribosomal binding affinity for particular mRNA sequences, or (2) these modifications might contribute to the formation of specialized ribosome populations that preferentially translate specific subsets of mRNAs. Future studies will be required to distinguish between these possibilities and fully elucidate the underlying molecular mechanisms.

Material and methods

Drosophila Strains

Fly stocks used in this study were maintained under standard culture conditions. We used the w^{1118} as the control strain. The following flies were obtained from Bloomington Stock Center: w^{1118} (Bl: 5905), *Mettl5*-Gal4 (Bl: 19514), *Repo*-Gal4 (Bl: 7415), *nSyb*-Gal4 (Bl: 51941), *pdf*-Gal4 (Bl: 41286), Clk^{JRK} (Bl: 80927), per^{01}(Bl: 80917), $Fmr1^{\Delta 50M}$(Bl: 6930), UAS-*Trmt112*RNAi (VDRC: 101515), UAS-DenMark,UAS-*syt*.eGFP (Bl: 33064), UAS-GFPstinger (from Yi Rao's lab), UAS-*Fmr1* (Bl: 6931), UAS-*Mettl5* (FlyORF: F000760) are from Fly ORF collection. UAS-*Mettl5m*-3HA (generated in this study).

$Mettl5^{1bp}$ and $Mettl5^{9bp}$ mutants were generated by the CRISPR/Cas system as described previously (Cheng et al., 2020). The target gRNA was designed with an online tool: *http://tools.flycrispr.molbio.wisc.edu/targetFinder/*. A target sequence was chosen that has the sequence of 5'- GAGTGGGGTACTGTTCCAAC**AGG** with the PAM sequence in bold. Mutations were verified by genomic PCR and sequencing.

Sleep behavior assays

All sleep assays were conducted in a controlled environment incubator maintained at 25 ± 1°C with 60% ± 5% relative humidity. We maintained a 12:12 light-dark cycle with lights on at ZT0 (06:30) and off at ZT12 (18:30). Fly activity was monitored using the Drosophila Activity Monitoring System (Trikinetics, Waltham, MA). Following a 2-day acclimation period, we recorded locomotor activity at 1-minute intervals for 3 consecutive days. Data analysis was performed using pysolo (Gilestro and Cirelli, 2009), with sleep defined as ≥5 minutes of continuous inactivity.

Mechanical sleep deprivation was performed using the SNAP method to keep flies awake for 12 h overnight (Shaw et al., 2002). Sleep deprivation is applied by mechanical stimuli using a timer-controlled rotating shaker. The intensity of stimuli was 1500 rpm once every minute (2 s/1 min) (Shimizu et al., 2008). Baseline sleep was established from 24-hour recordings prior to deprivation. Sleep loss and recovery were quantified according to previous publication (Cirelli C et al., 2005).

Regarding the 'awake %' metric, it indicates that at specific time points (e.g., ZT14), the percentage of awake fruit fly population at that moment. At ZT19, we evaluated arousal thresholds by administering a standardized gentle mechanical stimulus. Responsiveness was determined by monitoring activity for 1 minutes post-stimulation. Flies showing no activity during this window were scored as non-responsive. We calculated arousal percentages from the proportion of flies that awakened in response to stimulation.

Circadian rhythm of individual male flies was measured using the Drosophila Activity Monitoring (DAM) System (Trikinetics). Male flies were loaded individually into glass tubes with a length of 65 mm and an inner diameter of 5 mm. The tubes contained standard cornmeal fly food at one end

and were sealed with a cotton stopper at the other end. The flies were entrained to a 12 h light/12 h dark cycle for 3 days and then released to constant darkness for at least six days to measure their rhythmicity.Data analysis is done on a Macintosh computer running the FaasX (Fly activity analysis suite) software.

Statistical analysis

All statistical analyses were performed using GraphPad Prism 5 software. For sleep parameter comparisons, we used nonparametric tests including the two-tailed Mann-Whitney test for pairwise comparisons and one-way ANOVA with Tukey's post hoc test for multiple comparisons. qPCR data were analyzed using unpaired Student's t-tests, while lifespan data were evaluated with Log-rank (Mantel-Cox) tests. The specific statistical test used for each experiment is indicated in the corresponding figure. In all analyses, a p-value of less than 0.05 was considered statistically significant.

Quantitative PCR

Total RNA was extracted from cells and tissues using the TRNzol Universal Reagent (Tiangen #DP4-02). For cDNA synthesis, we employed the PrimeScript RT reagent Kit with gDNA Eraser (TAKARA #RR047A) following the manufacturer's protocol. Quantitative PCR was carried out using SuperReal PreMix Plus (SYBR Green) (Tiangen #DP4-02). *RP49* served as the endogenous reference gene for normalization across samples. All experiments included three independent biological replicates to ensure reproducibility. The primers used in this experiment are *RP49*-F: CGGTTACGG ATCGAACAAGC; *RP49*-R: CTTGCGCTTCTTGGAGGAGA; *Mettl5*-F: CGGTTTCTGGAGGTGGC; *Mettl5*-R: G CTGGCGTCGATGTTGTAC..

Imaging and analysis of axon volume

We quantified small LNvs axon volume using ImageJ's Object Counter 3D plugin to measure pixel counts from raw images. Image processing involved applying a standardized threshold that clearly visualized intact axons in control samples. For consistent measurements, we specifically analyzed the axon span between the first axonal bifurcation and the terminal tip, as indicated by the white rectangular markers in Figure 8.

Sample collection and library construction for Ribo-seq and RNAseq

For sample collection, w^{1118} and $Mettl5^{1bp}$ *Drosophila* were harvested at ZT15, immediately transferred to centrifuge tubes, and flash-frozen in liquid nitrogen. Fly heads were subsequently separated and collected while frozen, with three biological replicates prepared for each genotype. Each sample was equally divided for parallel RNA-seq and Ribo-seq analyses. For Ribo-seq library preparation, samples were lysed in buffer containing 50 mg/mL cycloheximide (Novogen, China) to preserve ribosome positioning, followed by RNase I digestion to generate ribosome-protected fragments (RPFs). Monosomes were isolated using MicroSpin S-400 HR size-exclusion chromatography, followed by rRNA depletion and PAGE purification to select 20-38 nt RPFs. Purified fragments underwent end repair, adapter ligation, reverse transcription, and PCR amplification before Illumina PE150 sequencing. For RNA-seq, total RNA was extracted using TRIzol reagent, with cDNA libraries prepared and sequenced using Illumina PE150 by Novogen. Raw sequencing data in FASTQ format were processed to remove adapter sequences, reads containing N bases, and low-quality reads, while simultaneously calculating Q20/Q30 scores and GC content to generate clean reads for downstream analysis.

RNA-seq analysis

We performed genome alignment and transcriptome analysis using the following pipeline: First, we built a Hisat2 index (v2.0.5) for the Drosophila melanogaster reference genome (dm6 assembly). Clean paired-end reads were then aligned to this reference using Hisat2 (v2.0.5) (Kim et al., 2019). The resulting alignments were processed using StringTie (v1.3.3b) (Pertea et al.,

2015) for reference-based transcript assembly. For gene-level quantification, we used FeatureCounts (v1.5.0) (Liao et al., 2014) to count reads mapped to each annotated gene. Differential expression analysis between $w^{1118}$and $Mettl5^{1bp}$ was conducted with DESeq2 (v1.20.0) (Pertea et al., 2015), with genes meeting both criteria (adjusted p-value < 0.05 and absolute log2 fold change ≥ 1) considered statistically significant.

Ribo-seq analysis

We implemented a comprehensive Ribo-seq analysis pipeline beginning with quality filtering using Bowtie (Liao et al., 2014) to remove reads aligning to non-coding RNAs (rRNA, tRNA, snoRNA, snRNA from FlyBase Release 6.13) with a 2-mismatch allowance (-v 2). The remaining ribosome-protected fragments (RPFs) were mapped to the *Drosophila melanogaster* genome (FlyBase Release 6.13) using STAR (v2.7.3a) (Dobin et al., 2013), followed by transcript-level alignment to protein-coding sequences using Bowtie (v1.2.2) (Langmead et al., 2009) with parameters "-a -v 2". CDS-aligned RPFs were quantified using featureCounts (Subread v1.6.3) and normalized as RPKM. Differential expression analysis was performed with DESeq2 (v1.14.1) (Love et al., 2014) using thresholds of $|\log2FC| \geq 0.265$ and padj < 0.05, while translation efficiency differences were assessed using RiboDiff. Data quality was verified through riboWaltz (v1.1.0) (Lauria et al., 2018) for 3-nt periodicity and reading frame analysis, with Ribocode (Xiao et al., 2018) employed for P-site positioning and uORF motif analysis. Functional enrichment analyses (GO, KEGG, GSEA) were conducted using clusterProfiler (v4.5.2.002) (Wu et al., 2021), with results visualized through ggplot2-generated plots and GO term simplification performed using SimplifyEnrichment (Gu and Hübschmann, 2022).

Immunofluorescence experiments

We performed immunofluorescence staining on 7-15 days old adult flies (unless otherwise specified). Flies were anesthetized with CO_2 and dissected in ice-cold 0.03% PBST (1× PBS with 0.03% Triton X-100; Sigma, T9284). Samples were fixed in 2% paraformaldehyde (PFA) for 55 minutes at room temperature (RT), followed by four 15-minute washes in 0.03% PBST at RT. After blocking overnight at 4°C in 10% Normal Goat Serum (NGS; in 1× PBS with 2% Triton), samples were incubated with primary antibodies for 24 hours at 4°C. Primary antibodies included rat anti-Elav (DSHB, 9F8A9; 1:200) and mouse anti-Repo (DSHB, 8D12; 1:200), diluted in antibody buffer (1.25% PBST, 1% NGS). Following four 15-minute washes in 1× PBS with 1% Triton at RT, samples were incubated overnight at 4°C with secondary antibodies: Alexa Fluor™ 568 (Thermo Fisher, A11004; 1:200) and Alexa Fluor™ 647 (Thermo Fisher, A21247; 1:200). After four additional 15-minute washes in 1× PBS with 1% Triton at RT, samples were mounted using DAPI-containing antifade mounting medium (Solarbio, S2110).

Images were acquired using a Leica SP8 confocal microscope with LAS X software, applying auto Z-brightness correction when needed for signal uniformity. Images were processed in Adobe Photoshop CS6 and figures assembled in Adobe Illustrator 2020. PDF immunofluorescence followed the same protocol. All experiments included ≥3 biological replicates, each containing ≥10 flies. Fluorescence intensity was quantified using ImageJ.

Western Blotting

Protein samples were prepared by homogenizing approximately 30 fly heads in RIPA lysis buffer (150 mM NaCl, 1.0% NP-40, 0.5% sodium deoxycholate, 0.1% SDS, 50 mM Tris-HCl, pH 8.0) supplemented with protease (CW2200S) and phosphatase (CW2383S) inhibitor cocktails according to manufacturer specifications. Lysates were mixed with 2× SDS loading buffer, boiled at 100°C for 5 min, and immediately cooled on ice.

For immunoblotting, membranes were probed with rabbit anti-PER primary antibody (1:5000 dilution; kindly provided by Dr. Jeffrey Price's laboratory, University of Missouri-Kansas City) overnight at 4°C, followed by incubation with HRP-conjugated goat anti-rabbit IgG secondary antibody (1:1500; ABclonal, AS014) for 4 hr at room temperature. Protein signals were detected

using ECL substrate (ABclonal, RM00021P) and imaged with an Amersham ImageQuant 800 system (GE Healthcare). Band intensities were quantified using ImageJ software, with three biological replicates performed for statistical reliability.

LC-MS/MS analysis of m^6A levels

Total RNA was isolated from cells and tissues using TRNzol Universal Reagent (Tiangen, #DP4-02). For 18S rRNA purification, we separated total RNA by polyacrylamide gel electrophoresis followed by gel extraction. Our analysis utilized ribonucleoside standards including adenosine (rA) and N6-methyladenosine (N6 mA), with a mobile phase consisting of methanol:ddH2O (v/v).

For each biological replicate, 1 μg of total RNA or purified 18S rRNA was digested to single nucleosides using Nucleoside Digestion Mix (NEB, #M0649). Proteins were precipitated by adding a 4:1 methanol:digest ratio and incubating at -20°C for 2 hours. Quantitative analysis was performed using multiple reaction monitoring (MRM) with the following transitions: 268.10275→136.0621 (rA), 282.11835→150.0774 (N6 mA).

Negative geotaxis RING assay

Climbing assays were performed following a 12-hour recovery period after CO2 anesthesia, using 200 flies per genotype distributed across 10 vials (20 flies/vial) marked at 90 mm height. Each assay consisted of three trials separated by 15-minute intervals, initiated by sharply tapping vials three times to induce negative geotaxis, with the number of flies reaching the 90 mm mark within 10 seconds recorded per trial. Five groups were tested per genotype (15 trials total). All assays were video recorded under standardized conditions with the camera positioned 20 cm from vials and uniform backlighting provided by a white open-faced box to ensure consistent imaging quality.

Supplementary figures

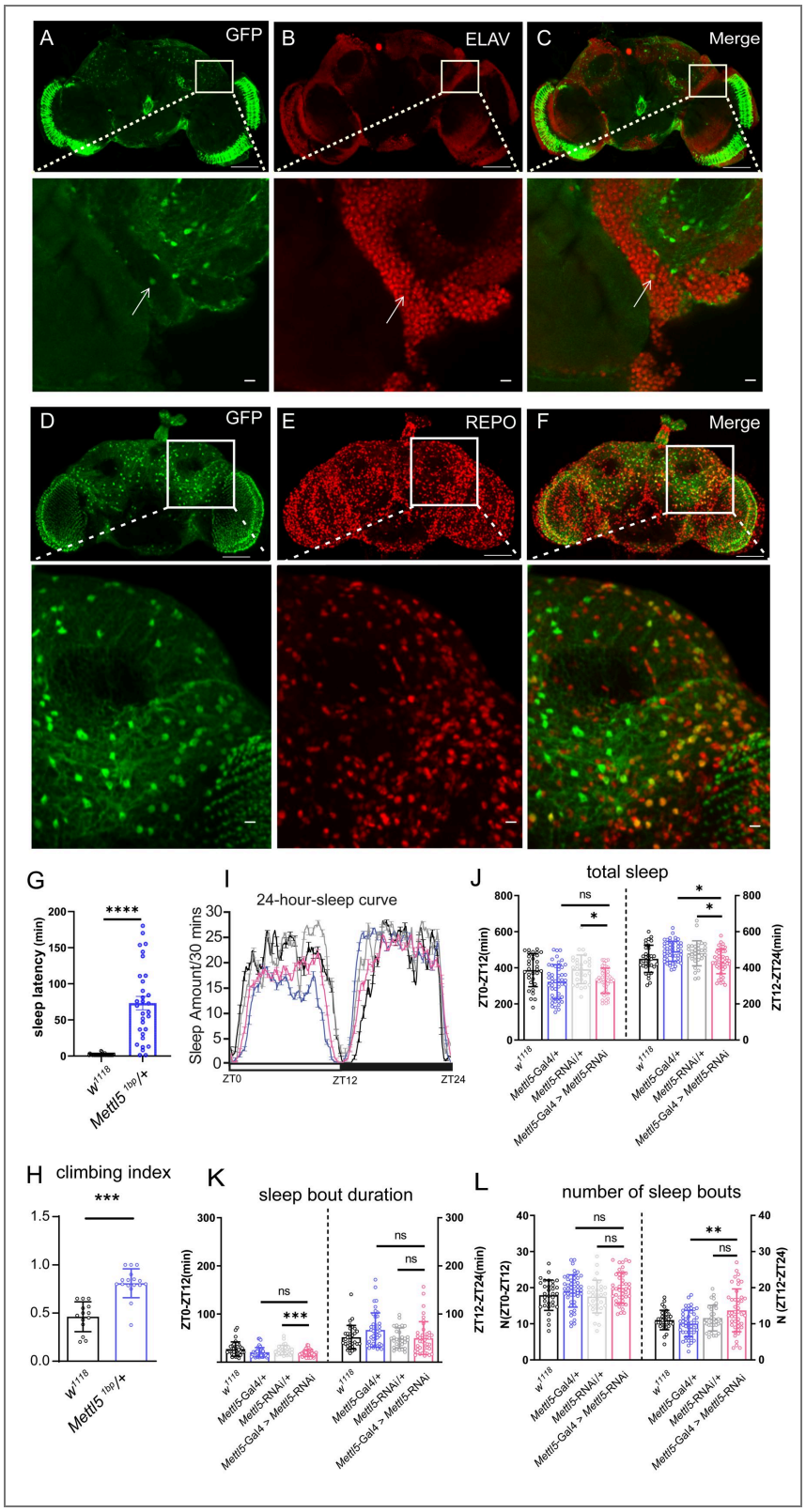

Figure S1. ***Mettl5*** **functions in a portion of neurons and glia.** (A-C) Colocalization of Mettl5-YFP with antibodies staining ELAV. Scale bar: 50 μm (main figures) and 20 μm (zoomed regions) (D-F) Colocalization of Mettl5-YFP with antibodies staining REPO. Scale bar: 50 μm (main figures) and 20 μm (zoomed regions). (G) Sleep latency. (H) Climbing index of *Mettl5*^{1bp} male flies and control flies. (I) Sleep curves throughout the day for *Mettl5*-RNAi and

control flies. (J) Total sleep for *Mettl5*-RNAi and control flies flies. (K) Sleep bout duration of *Mettl5*-RNAi and control flies. (L)Number of sleep bouts of *Mettl5*-RNAi and control flies. For statistical significance, * stands for $p<0.05$, ** stands for $p<0.01$, *** stands for $p<0.001$, *ns* stands for not significant

Figure S2. Quality control of RNA-seq and Ribo-seq samples.

(A, D) Meta analysis of gene expression data obtained from RNA-seq and Ribo-seq. (B, E) Principal component analysis (PCA) of different samples for RNA-seq and Ribo-seq. (C, F) Correlation heatmap of normalized RNA and RPFs values between every pair of samples. The color and size of dots represent the Pearson correlation coefficient.

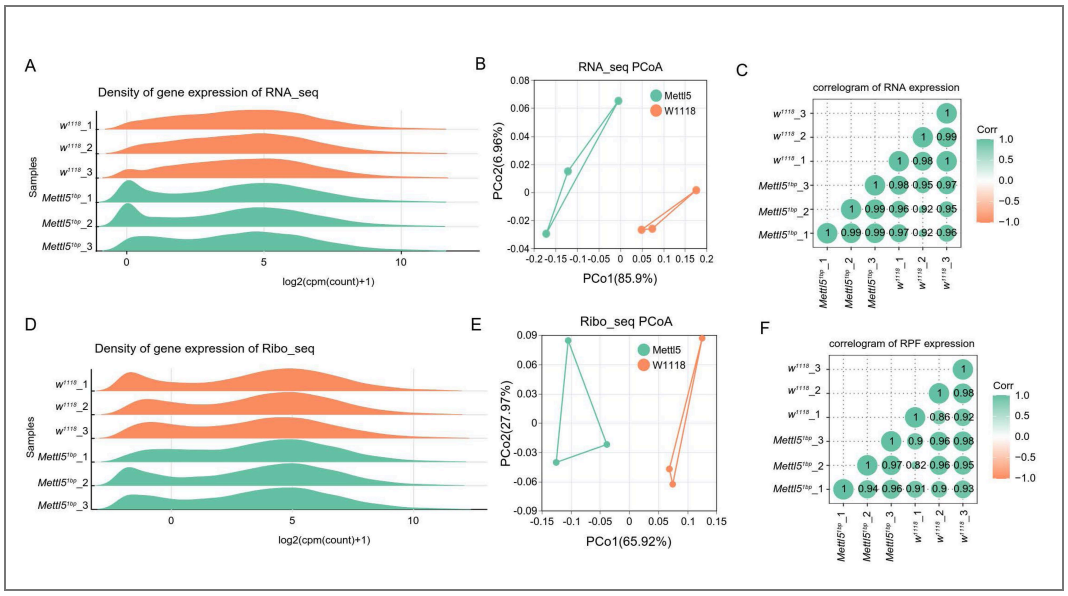

Figure S3. Heatmap of differentially expressed genes (DEGs) between *Mettl5*^{1bp} and *w*^{1118}.

Heatmap showing the top 100 significantly changed genes identified by RNA-seq (A) and Ribo-seq (B) in *Mettl5*^{1bp}. Red indicates increased expression, while blue indicates decreased expression.

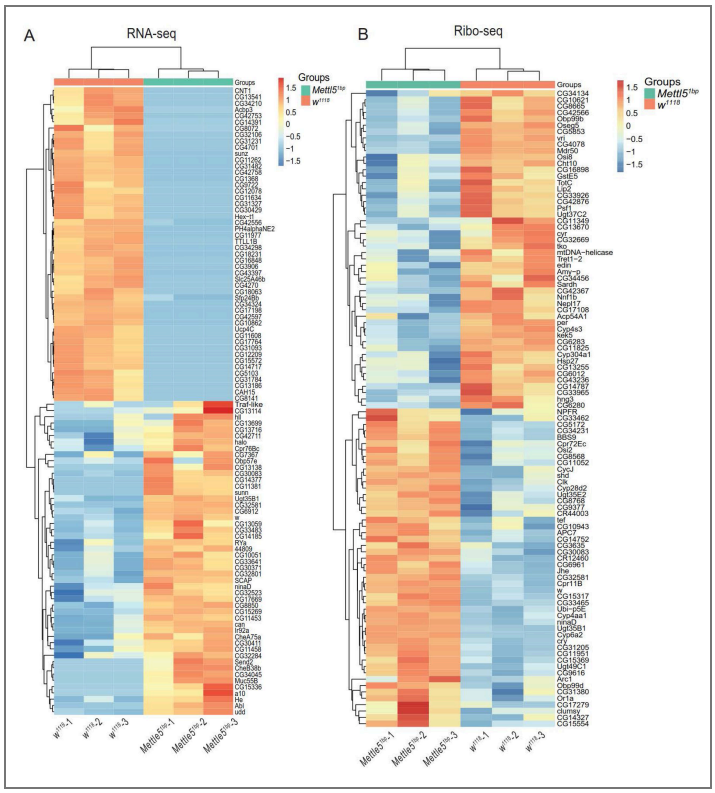

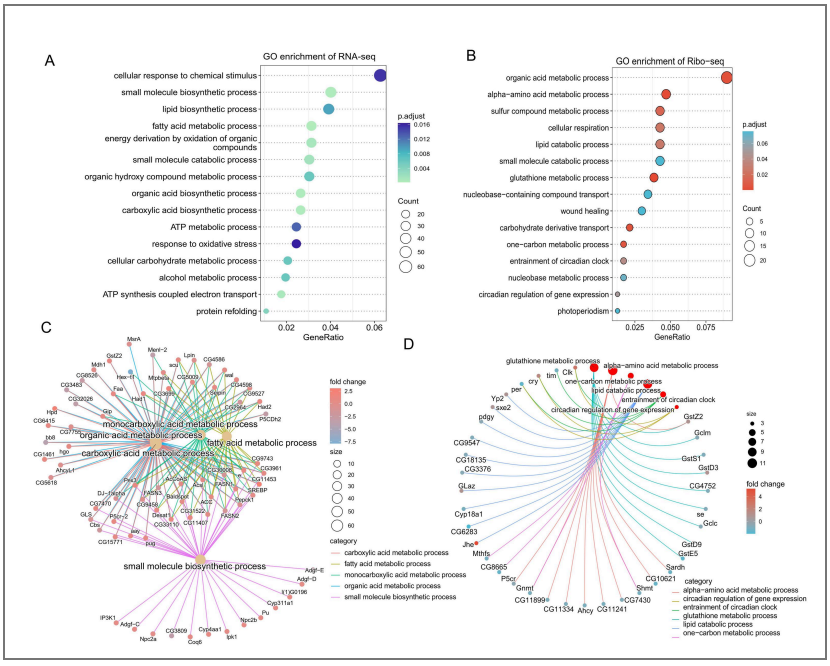

Figure S4. Enrichment analysis of differential expressed genes between *Mettl5*^{1bp} and *w*^{1118}.

(A-D) GO analysis performed on the differentially expressed genes revealed by RNA-seq (A, C) and Ribo-seq (B, D). The bubble chart shows the top 15 most significantly enriched categories under the themes of biological processes, cellular components and molecular functions. The circle color indicates the enrichment p.adjust, and the dot size indicates the number of differentially expressed genes in the functional class or pathway.

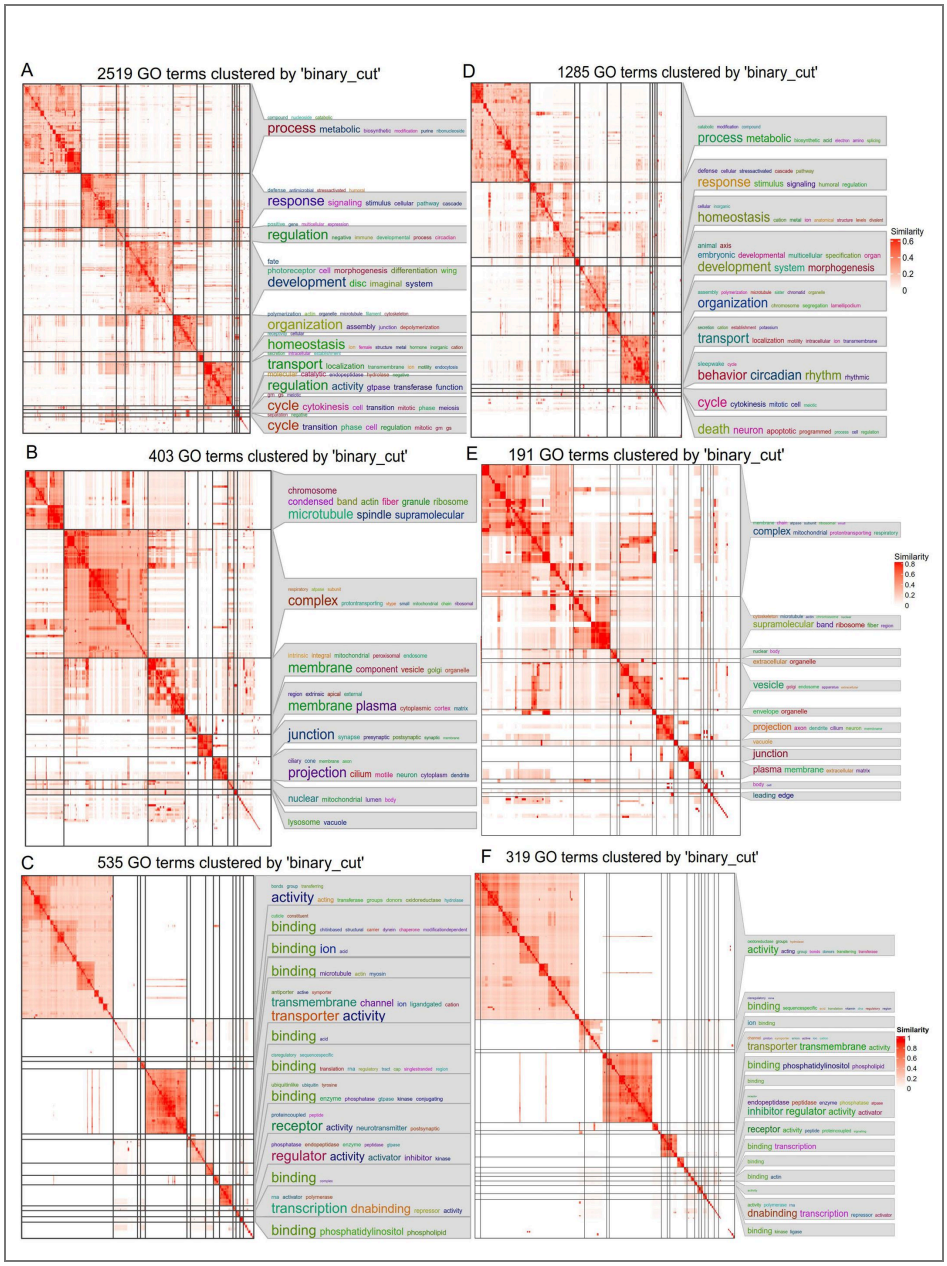

Figure S5. Simplified GO enrichment analysis for differentially expressed genes in RNA-seq and Ribo-seq.

GO enrichments for biological process (A, D), cellular components (B, E), and molecular function (C, F) were shown. The bottom right clusters, which lack word cloud annotations, include all other small clusters with fewer than 5 terms. The color shades represent the similarity of GO terms based on binary cut clustering.

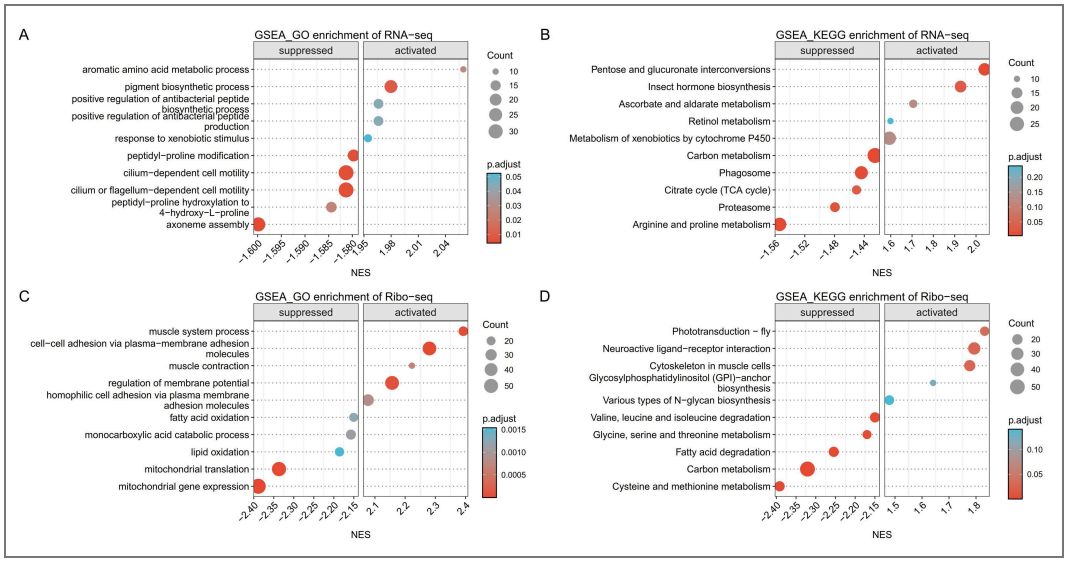

Figure S6. Gene set enrichment analysis (GSEA) for differentially expressed genes found in RNA-seq and Ribo-seq.

GSEA were performed on the differentially expressed genes identified in RNA-seq (A, B) and Ribo-seq (C, D). The top 5 terms or pathways found in GSEA based on GO (A, C) and KEGG (B, D) databases are shown. Genes were sorted according to their signed NES values. The circle color indicates the enrichment p.adjust, and the dot size indicates the number of differentially expressed genes in the respective functional class or pathway.

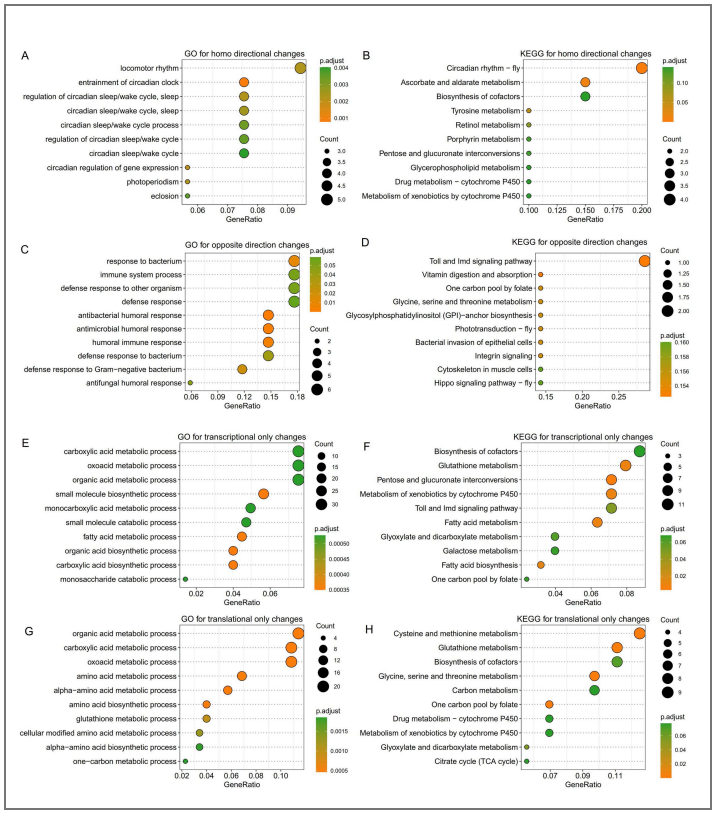

Figure S7. GO and KEGG enrichment analysis of genes that were significantly changed at both transcriptional and translational levels (showed in figure3L).

(A, B) Top 10 GO and KEGG terms for genes with the same direction of change at transcriptional and translational levels. (C, D) Top 10 GO and KEGG terms for genes with the opposite direction of change at transcriptional and translational levels. (E, F) Top 10 GO terms for genes that were only changed at the transcriptional level; (G, H) Top 10 GO terms for genes that were only changed at the translational level. The circle color indicates the enrichment p.adjust, and the dot size indicates the number of differentially expressed genes in the respective functional class or pathway. Changes with $|\log_2$ (fold change) $|\geq$ 0.265 of translational levels and $|\log_2$(fold change) $|\geq 1$ of transcriptional levels were considered significant.

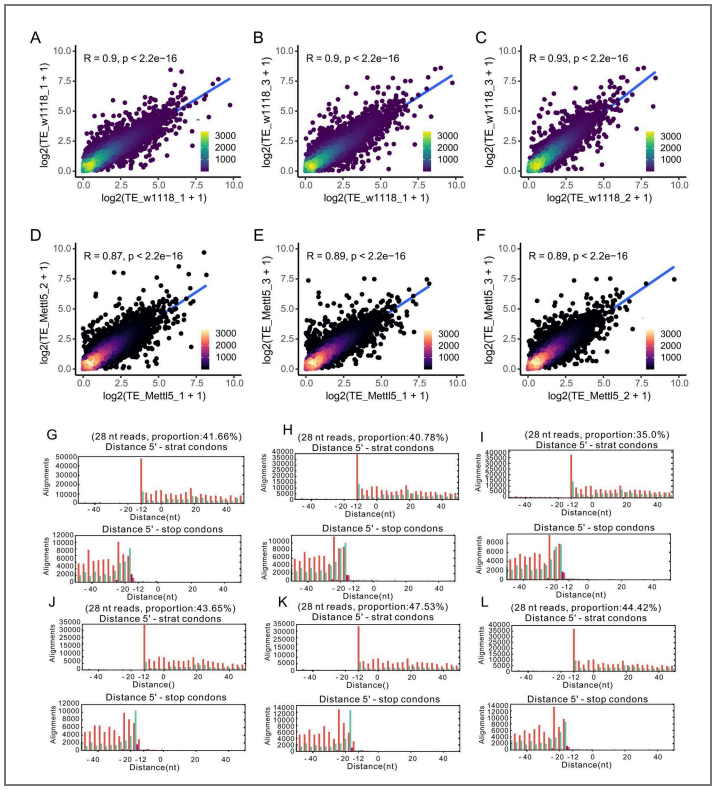

Figure S8. TE correlation and P-site offsets

(A-F) TE correlation between the three biological replicates of two group showing high reproducibility. Different colors represent the density distribution of different translated genes. (G-L) Metagene analysis of individual 28nt reads mapped to their 5′ ends to determine P-site offsets. The distribution of 28nt RPF reads around the ribosomal P site in w^{1118} (G-I) and *Mettl5* (J-L). The horizontal axis represents the distance from the start-codon or stop-codon, and the vertical axis represents the read counts. The P-site positions are colored according to the reading frame.

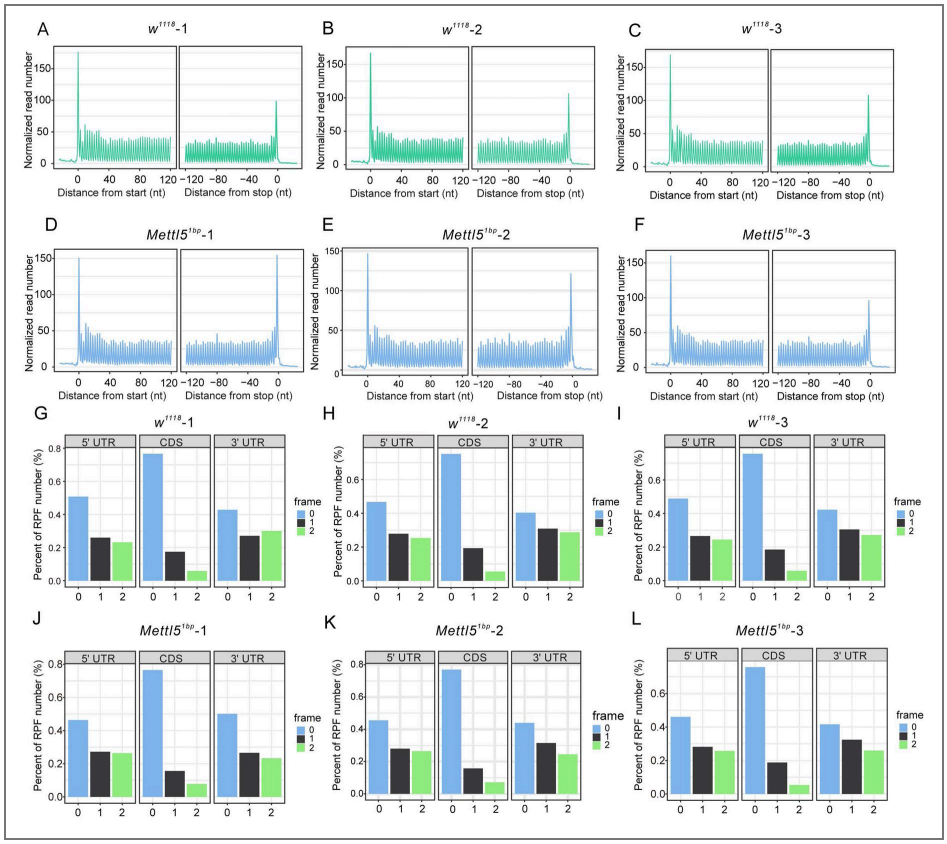

Figure S9. Global scan of RPFs distribution

(A-F) Distribution of RPFs periodicity among translation start codons and translation end codons in w^{1118} (A-C) and $Mettl5^{1bp}$(D-F). (G-L) Distribution of RPFs on different coding frames, including frame 0, frame 1 and frame 2, for the 5'UTR, CDS and 3'UTR in w^{1118} (G-I) and $Mettl5^{1bp}$ (J-L). The plot illustrates the distribution of ribosome-protected fragments (RPFs) across different coding frames (frame 0, frame 1, and frame 2) on the x-axis, with the y-axis representing the percentage of RPFs in each coding frame.

Figure S10. Ribo-seq has revealed that the *Mettl5*^{1bp} leads to changes in global translation features.

(A) The distribution of RPF length among different samples in *Mettl5*^{1bp}and *w*^{1118} was compared. (B) A comparison was made between *Mettl5*^{1bp} and *w*^{1118}regarding the statistics on active translated ORFs. The distribution of different types of ORFs based on their relative location to associated coding sequences (CDS) was illustrated in the comparison between *Mettl5*^{1bp} and *w*^{1118}. The categories include “annotated” (ORFs that overlap with annotated CDS and have the same stop codon as the annotated CDS), “uORF” (ORFs located upstream of annotated CDS, not overlapping annotated CDS), “dORF” (ORFs located downstream of annotated CDS, not overlapping annotated CDS), “Overlap_uORF” (ORFs located upstream of annotated CDS, overlapping annotated CDS), “Overlap_dORF” (ORFs located downstream of annotated CDS, overlapping annotated CDS), “Internal” (ORFs located within annotated CDS but in a different frame relative to the annotated CDS), and “novel” (ORFs located in non-coding genes or non-coding transcripts of coding genes). The percentages of each ORF category were compared between *Mettl5*^{1bp} and *w*^{1118}, providing insights into the differences in ORF distribution between the two analyzed samples. (C) A comparison was made between *Mettl5*^{1bp} and *w*^{1118} regarding the length of translated and untranslated uORFs. (D) The count of dORFs was compared between *Mettl5*^{1bp} and *w*^{1118}. (E) The count of translated uORFs was compared between *Mettl5*^{1bp} and *w*^{1118}. (F, G) Motif analysis was performed separately on the translated and untranslated uORFs between *w*^{1118} and *Mettl5*^{1bp}. (H) The correlation of codon occupancy (A-site) between *Mettl5*^{1bp} and *w*^{1118} was analyzed. (I-L) The cumulative changes in RPFs for codon UCC (I), GAC (J), GAU (K) and amino acid ASP (L) were compared between *Mettl5*^{1bp}and *w*^{1118}. The statistical analysis was performed using the Kolmogorov-Smirnov test (KS test). (M-O) A metagene plot was generated for RPFs on whole CDS region and around the CDS start and end regions in group case study. The CDS was divided into 100 equal bins.

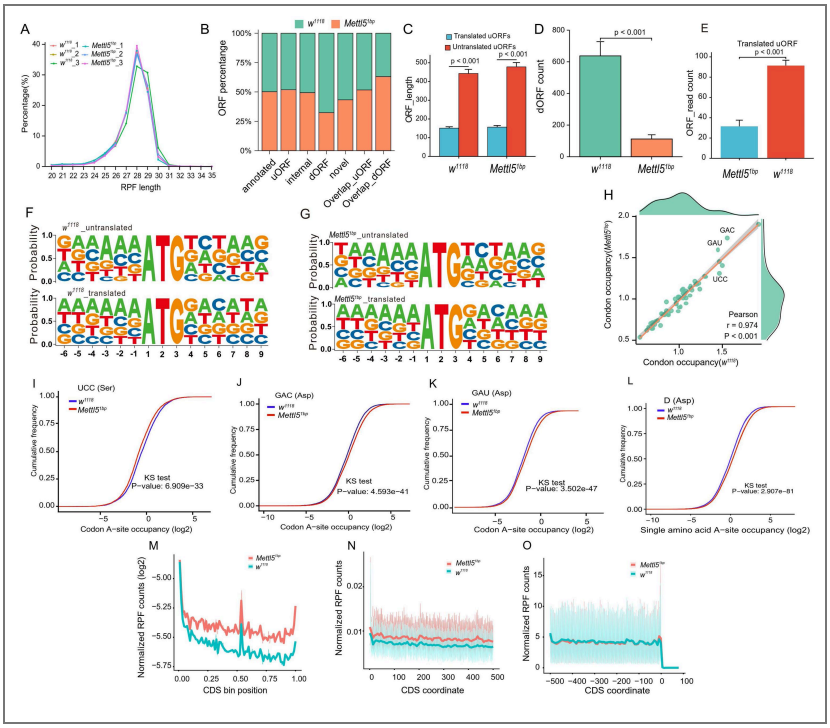

Figure S11. Morphology of clock neurons in *Mettl5* mutant.

Ventral lateral neurons labeled by PDF staining in *Mettl5*^{1bp} and control flies across different time points.

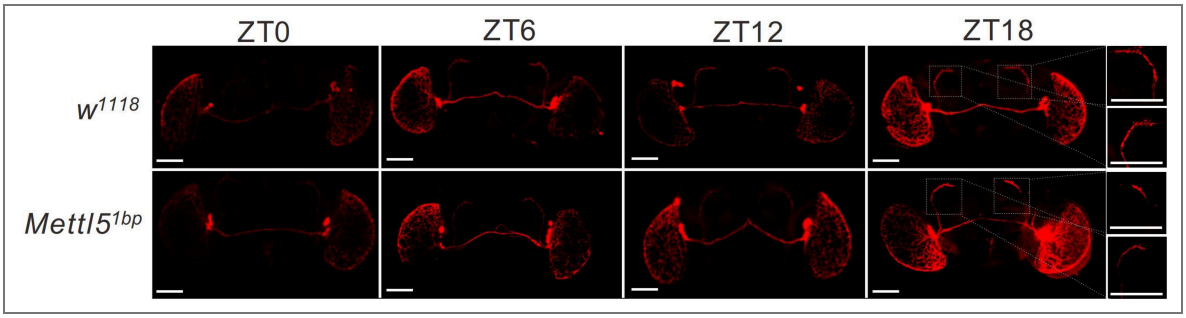

Data availability

The RNA-seq and Ribo-seq data from this publication have been deposited to the NCBI bioproject database *https://www.ncbi.nlm.nih.gov/bioproject/* and assigned the identifier PRJNA994860.

Acknowledgements

This work was supported by National Natural Science Foundation of China (Grant No. 32070492 and 32122017) to Juan Du. We would also like to acknowledge the 2115 Talent Development Program of China Agricultural University.

Additional information

Author contributions

XY, XW and TF designed and performed the experiments, analyzed the data and wrote the manuscript. XY performed the bioinformatics analysis, analyzed the data and edited the manuscript. YR analyzed data and edited the manuscript. JD designed experiments, analyzed data, wrote and edited the manuscript. All authors have read and approved the final manuscript.

Funding

Funder	Grant reference number	Author
MOST | National Natural Science Foundation of China (NSFC)	32070492	Juan Du
MOST | National Natural Science Foundation of China (NSFC)	32122017	Juan Du

Author ORCID iDs

Xingzhuo Yang: https://orcid.org/0009-0000-0025-5503
Yikang S Rong: https://orcid.org/0000-0002-9787-9669
Juan Du: https://orcid.org/0000-0002-1850-3613

References

Anafi RC, Kayser MS, Raizen DM (2019) Exploring phylogeny to find the function of sleep. *Nature Reviews Neuroscience* **20**:109-116 https://doi.org/10.1038/s41583-018-0098-9 | PubMed

Brüning F, Noya SB, Bange T, Koutsouli S, Rudolph JD, Tyagarajan SK, Cox J, Mann M, Brown SA, Robles MS (2019) Sleep-wake cycles drive daily dynamics of synaptic phosphorylation. *Science* **366**:eaav3617 https://doi.org/10.1126/science.aav3617 | PubMed

Bushey D, Tononi G, Cirelli C (2011) Sleep and synaptic homeostasis: structural evidence in *Drosophila*. *Science* **332**:1576-1581 https://doi.org/10.1126/science.1202839 | PubMed

Cheng L, Zhang Y, Zhang Y, Chen T, Xu YZ, Rong YS (2020) Loss of the RNA trimethylguanosine cap is compatible with nuclear accumulation of spliceosomal snRNAs but not pre-mRNA splicing or snRNA processing during animal development. *PLoS Genetics* **16**:e1009098 https://doi.org/10.1371/journal.pgen.1009098 | PubMed

Chiu JC, Vanselow JT, Kramer A, Edery I (2008) The phosphooccupancy of an atypical SLIMB-binding site on PERIOD that is phosphorylated by DOUBLETIME controls the pace of the clock. *Genes Dev* **22**:1758-1772 https://doi.org/10.1101/gad.1682708

Cirelli C, Bushey D, Hill S, Huber R, Kreber R, Ganetzky B, Tononi G (2005) Reduced sleep in Drosophila Shaker mutants. *Nature* **434**:1087-92 https://doi.org/10.1038/nature03486 | PubMed

Costa RO, Martins H, Martins LF, Cwetsch AW, Mele M, Pedro JR, Tomé D, Jeon NL, Cancedda L, Jaffrey SR, *et al.* (2019) Synaptogenesis stimulates a proteasome-mediated ribosome reduction in axons. *Cell Reports* **28**:864-876 https://doi.org/10.1016/j.celrep.2019.06.080 | PubMed

Desvergne A, Ugarte N, Radjei S, Gareil M, Petropoulos I, Friguet B (2016) Circadian modulation of proteasome activity and accumulation of oxidized protein in human embryonic kidney HEK 293 cells and primary dermal fibroblasts. *Free Radical Biology and Medicine* **94**:195-207 https://doi.org/10.1016/j.freeradbiomed.2016.02.037 | PubMed

Dobin A, Davis CA, Schlesinger F, Drenkow J, Zaleski C, Jha S, Batut P, Chaisson M, Gingeras TR (2013) STAR: ultrafast universal RNA-seq aligner. *Bioinformatics* **29**:15-21 https://doi.org/10.1093/bioinformatics/bts635 | PubMed

Du J, Lv P, Fu T, Wei Y, Zhao Z. (2021) Regulation of sleep in *Drosophila melanogaster*. *Advances in Insect Physiology* **60**:119-168

El-Brolosy MA, Kontarakis Z, Rossi A, Kuenne C, Gunther S, Fukuda N, Kikhi K, Boezio GLM, Takacs CM, Lai SL (2019) Genetic compensation triggered by mutant mRNA degradation. *Nature* **568**:193-197 https://doi.org/10.1038/s41586-019-1064-z | PubMed

Fernández-Cruz I, Sánchez-Díaz I, Narváez-Padilla V, Reynaud E (2020) Rpt2 proteasome subunit reduction causes Parkinson's disease like symptoms in *Drosophila*. *IBRO Reports* **9**:65-77 https://doi.org/10.1016/j.ibror.2020.07.001 | PubMed

Fu J, Murphy KA, Zhou M, Li YH, Lam VH, Tabuloc CA, Chiu JC, Liu Y (2016) Codon usage affects the structure and function of the *Drosophila* circadian clock protein PERIOD. *Genes & Development* **30**:1761-75 https://doi.org/10.1101/gad.281030.116 | PubMed

Galimberti V, Kinor N, Shav-Tal Y, Biggiogera M, Brüning A (2016) The stress-inducible transcription factor ATF4 accumulates at specific rRNA-processing nucleolar regions after proteasome inhibition. *European Journal of Cell Biolog* **95**:389-400 https://doi.org/10.1016/j.ejcb.2016.08.002 | PubMed

Gilestro GF, Tononi G, Cirelli C (2009) Widespread changes in synaptic markers as a function of sleep and wakefulness in *Drosophila*. *Science* **324**:109-112 https://doi.org/10.1126/science.1166673 | PubMed

Gilestro GF, Cirelli C (2009) pySolo: a complete suite for sleep analysis in Drosophila. *Bioinformatics* **25**:1466-1467 https://doi.org/10.1093/bioinformatics/btp237 | PubMed

Grima B, Lamouroux A, Chélot E, Papin C, Limbourg-Bouchon B, Rouyer F (2002) The F-box protein slimb controls the levels of clock proteins period and timeless. *Nature* **420**:178-82 https://doi.org/10.1038/nature01122 | PubMed

Gu Z, Hübschmann D (2022) simplifyEnrichment: A bioconductor package for clustering and visualizing functional enrichment results. *Genomics Proteomics Bioinformatics* **21**:190-202 https://doi.org/10.1016/j.gpb.2022.04.008 | PubMed

Huang S, Piao C, Beuschel CB, Götz T, Sigrist SJ (2020) Presynaptic active zone plasticity encodes sleep need in Drosophila. *Current Biology* **30**:1077-1091 https://doi.org/10.1016/j.cub.2020.01.019 | PubMed

Hwangbo DS, Kwon YJ, Iwanaszko M, Jiang P, Abbasi L, Wright N, Alli S, Hutchison AL, Dinner AR, Braun RI, *et al.* (2023) Dietary restriction impacts peripheral circadian clock output important for longevity in *Drosophila*. *eLife* **12**:RP86191 https://doi.org/10.7554/eLife.86191

Iyer LM, Zhang D, Aravind L (2016) Adenine methylation in eukaryotes: Apprehending the complex evolutionary history and functional potential of an epigenetic modification. *Bioessays* **38**:27-40 https://doi.org/10.1002/bies.201500104 | PubMed

Kapetanou M, Athanasopoulou S, Gonos ES (2022) Transcriptional regulatory networks of the proteasome in mammalian systems. *IUBMB Life* **74**:41-52 https://doi.org/10.1002/iub.2586 | PubMed

Kim D, Paggi JM, Park C, Bennett C, Salzberg SL (2019) Graph-based genome alignment and genotyping with HISAT2 and HISAT-genotype. *Nature Biotechnology* **37**:907-915 https://doi.org/10.1038/s41587-019-0201-4 | PubMed

Ko HW, Jiang J, Edery I (2002) Role for Slimb in the degradation of Drosophila period protein phosphorylated by doubletime. *Nature* **420**:673-678 https://doi.org/10.1038/nature01272 | PubMed

Langmead B, Trapnell C, Pop M, Salzberg SL (2009) Ultrafast and memory-efficient alignment of short DNA sequences to the human genome. *Genome Biology* **10**:R25 https://doi.org/10.1186/gb-2009-10-3-r25 | PubMed

Lauria F, Tebaldi T, Bernabò P, Groen EJN, Gillingwater TH, Viero G (2018) riboWaltz: Optimization of ribosome P-site positioning in ribosome profiling data. *PLoS Computational Biology* **14**:e1006169 https://doi.org/10.1371/journal.pcbi.1006169 | PubMed

Leismann J, Spagnuolo M, Pradhan M, Wacheul L, Vu MA, Musheev M, Mier P, Andrade-Navarro MA, Graille M, Niehrs C, *et al.* (2020) The 18S ribosomal RNA m^6A methyltransferase *Mettl5* is required for normal walking behavior in *Drosophila*. *EMBO Reports* **21**:e49443 https://doi.org/10.15252/embr.201949443 | PubMed

Liao Y, Smyth GK, Shi W (2014) featureCounts: an efficient general purpose program for assigning sequence reads to genomic features. *Bioinformatics* **30**:923-930 https://doi.org/10.1093/bioinformatics/btt656 | PubMed

Liu ZW, Faraguna U, Cirelli C, Tononi G, Gao XB (2010) Direct evidence for wake-related increases and sleep-related decreases in synaptic strength in rodent cortex. *Journal Of Neuroscience* **30**:8671-8675 https://doi.org/10.1523/jneurosci.1409-10.2010 | PubMed

López-Varea A, Vega-Cuesta P, Ruiz-Gómez A, Ostalé CM, Molnar C, Hevia CF, Martín M, Organista MF, de Celis J, Culí J, *et al.* (2021) Genome-wide phenotypic RNAi screen in the Drosophila wing: phenotypic description of functional classes. *G3* **11**:jkab349 https://doi.org/10.1093/g3journal/jkab349 | PubMed

Love MI, Huber W, Anders S (2014) Moderated estimation of fold change and dispersion for RNA-seq data with DESeq2. *Genome Biology* **15**:550 https://doi.org/10.1186/s13059-014-0550-8 | PubMed

Lyons LC, Vanrobaeys Y, Abel T (2023) Sleep and memory: The impact of sleep deprivation on transcription, translational control, and protein synthesis in the brain. *Journal Of Neurochemistry* **166**:24-46 https://doi.org/10.1111/jnc.15787 | PubMed

Ma Z, Zhu P, Shi H, Guo L, Zhang Q, Chen Y, Chen S, Zhang Z, Peng J, Chen J (2019) PTC-bearing mRNA elicits a genetic compensation response via Upf3a and COMPASS components. *Nature* **568**:259-263 https://doi.org/10.1038/s41586-019-1057-y | PubMed

Noya SB, Colameo D, Brüning F, Spinnler A, Mircsof D, Opitz L, Mann M, Tyagarajan SK, Robles MS, Brown SA (2019) The forebrain synaptic transcriptome is organized by clocks but its proteome is driven by sleep. *Science* **366**:eaav2642 https://doi.org/10.1126/science.aav2642 | PubMed

Palanca A, Casafont I, Berciano MT, Lafarga M (2014) Reactive nucleolar and Cajal body responses to proteasome inhibition in sensory ganglion neurons. *Biochimica et Biophysica Acta* **1842**:848-859 https://doi.org/10.1016/j.bbadis.2013.11.016 | PubMed

Patop IL, Anduaga AM, Bussi IL, Ceriani MF, Kadener S (2023) Organismal landscape of clock cells and circadian gene expression in *Drosophila*. *bioRxiv* https://doi.org/10.1101/2023.05.23.542009 | PubMed

Peng H, Chen B, Wei W, Guo S, Han H, Yang C, Ma J, Wang L, Peng S, Kuang M, *et al.* (2022) N^6-methyladenosine (m^6A) in 18S rRNA promotes fatty acid metabolism and oncogenic transformation. *Nature Metabolism* **4**:1041-54 https://doi.org/10.1038/s42255-022-00622-9 | PubMed

Pertea M, Pertea GM, Antonescu CM, Chang TC, Mendell JT, Salzberg SL (2015) StringTie enables improved reconstruction of a transcriptome from RNA-seq reads. *Nature Biotechnology* **33**:290-295 https://doi.org/10.1038/nbt.3122 | PubMed

Philpott JM, Freeberg AM, Park J, Lee K, Ricci CG, Hunt SR, Narasimamurthy R, Segal DH, Robles R, Cai Y, *et al.* (2023) PERIOD phosphorylation leads to feedback inhibition of CK1 activity to control circadian period. *Molecular Cell* **83**:1677-1692 https://doi.org/10.1016/j.molcel.2023.04.019 | PubMed

Richard EM, Polla DL, Assir MZ, Contreras M, Shahzad M, Khan AA, Razzaq A, Akram J, Tarar MN, Blanpied TA, *et al.* (2019) Bi-allelic variants in METTL5 cause autosomal-recessive intellectual disability and microcephaly. *American Journal Of Human Genetics* **105**:869-878 https://doi.org/10.1016/j.ajhg.2019.09.007 | PubMed

Rong B, Zhang Q, Wan J, Xing S, Dai R, Li Y, Cai J, Xie J, Song Y, Chen J, *et al.* (2020) Ribosome 18S m^6A methyltransferase *METTL5* promotes translation initiation and breast cancer cell growth. *Cell Reports* **33**:108544 https://doi.org/10.1016/j.celrep.2020.108544 | PubMed

Rossi A, Kontarakis Z, Gerri C, Nolte H, Holper S, Kruger M, Stainier DY (2015) Genetic compensation induced by deleterious mutations but not gene knockdowns. *Nature* **524**:230-233 https://doi.org/10.1038/nature14580 | PubMed

Sepich-Poore C, Zheng Z, Schmitt E, Wen K, Zhang ZS, Cui XL, Dai Q, Zhu AC, Zhang L, Sanchez Castillo A, *et al.* (2022) The METTL5-TRMT112 N6-methyladenosine methyltransferase complex regulates mRNA translation via 18S rRNA methylation. *Journal Of Biological Chemistry* **298**:101590 https://doi.org/10.1016/j.jbc.2022.101590 | PubMed

Shaw PJ, Tononi G, Greenspan RJ, Robinson DF (2002) Stress response genes protect against lethal effects of sleep deprivation in *Drosophila*. *Nature* **417**:287-291 https://doi.org/10.1038/417287a | PubMed

Shimizu H, Shimoda M, Yamaguchi T, Seong KH, Okamura T, Ishii S (2008) *Drosophila* ATF-2 regulates sleep and locomotor activity in pacemaker neurons. *Molecular And Cellular Biology* **28**:6278-6289 https://doi.org/10.1128/mcb.02242-07 | PubMed

Simsek D, Tiu GC, Flynn RA, Byeon GW, Leppek K, Xu AF, Chang HY, Barna M (2017) The mammalian Ribo-interactome reveals ribosome functional diversity and heterogeneity. *Cell* **169**:1051-1065. https://doi.org/10.1016/j.cell.2017.05.022 | PubMed

Sun J, Zhou H, Chen Z, Zhang H, Cao Y, Yao X, Chen X, Liu B, Gao Z, Shen Y, *et al.* (2023) Altered m6A RNA methylation governs denervation-induced muscle atrophy by regulating ubiquitin proteasome pathway. *J Transl Med* **21**:845 https://doi.org/10.1186/s12967-023-04694-3 | PubMed

Teng X, Dayhoff-Brannigan M, Cheng WC, Gilbert CE, Sing CN, Diny NL, Wheelan SJ, Dunham MJ, Boeke JD, Pineda FJ (2013) Genome-wide consequences of deleting any single gene. *Molecular Cell* **52**:485-494 https://doi.org/10.1016/j.molcel.2013.09.026 | PubMed

Tononi G, Cirelli C (2006) Sleep function and synaptic homeostasis. *Sleep Medicine Reviews* **10**:49-62 https://doi.org/10.1016/j.smrv.2005.05.002 | PubMed

van Tran N, Ernst FGM, Hawley BR, Zorbas C, Ulryck N, Hackert P, Bohnsack KE, Bohnsack MT, Jaffrey SR, Graille M, *et al.* (2019) The human 18S rRNA m^6A methyltransferase METTL5 is stabilized by TRMT112. *Nucleic Acids Research* **47**:7719-7733 https://doi.org/10.1093/nar/gkz619 | PubMed

Vu V, Verster AJ, Schertzberg M, Chuluunbaatar T, Spensley M, Pajkic D, Hart GT, Moffat J, Fraser AG (2015) Natural variation in gene expression modulates the severity of mutant phenotypes. *Cell* **162**:391-402 https://doi.org/10.1016/j.cell.2015.06.037 | PubMed

Vyazovskiy VV, Cirelli C, Pfister-Genskow M, Faraguna U, Tononi G (2008) Molecular and electrophysiological evidence for net synaptic potentiation in wake and depression in sleep. *Nature Neuroscience* **11**:200-208 https://doi.org/10.1038/nn2035 | PubMed

Xiao Z, Huang R, Xing X, Chen Y, Deng H, Yang X (2018) De novo annotation and characterization of the translatome with ribosome profiling data. *Nucleic Acids Research* **46**:e61 https://doi.org/10.1093/nar/gky179 | PubMed

Wang L, Liang Y, Lin R, Xiong Q, Yu P, Ma J, Cheng M, Han H, Wang X, Wang G, *et al.* (2020) Mettl5 mediated 18S rRNA N6-methyladenosine (m^6A) modification controls stem cell fate determination and neural function. *Genes & Diseases* **9**:268-274 https://doi.org/10.1016/j.gendis.2020.07.004 |

PubMed

Wu T, Hu E, Xu S, Chen M, Guo P, Dai Z, Feng T, Zhou L, Tang W, Zhan L, *et al.* (2021) clusterProfiler 4.0: A universal enrichment tool for interpreting omics data. *Innovation* **2**:e100141 https://doi.org/10.1016/j.xinn.2021.100141 | PubMed

Zhang L, Hirano A, Hsu PK, Jones CR, Sakai N, Okuro M, McMahon T, Yamazaki M, Xu Y, Saigoh N, *et al.* (2016) A *PERIOD3* variant causes a circadian phenotype and is associated with a seasonal mood trait. *Proceedings of the National Academy of Sciences* **113**:E1536-44 https://doi.org/10.1073/pnas.1600039113 | PubMed

Xingzhuo Yang (2024) RNA-seq and Ribo-seq revealed the downstream events in Mettl5 mutation. NCBI BioProject. ID PRJNA994860 https://www.ncbi.nlm.nih.gov/bioproject/PRJNA994860

Peer reviews

Reviewer #1 (Public review):

Summary:

Here the authors attempted to test whether the function of Mettl5 in sleep regulation was conserved in Drosophila, and if so, by which molecular mechanisms. To do so they performed sleep analysis, as well as RNA-seq and ribo-seq in order to identify the downstream targets. They found that the loss of one copy of Mettl5 affects sleep, and that its catalytic activity is important for this function. Transcriptional and proteomic analyses show that multiple pathways were altered, including the clock signaling pathway and the proteasome. Based on these changes the authors propose that Mettl5 modulate sleep through regulation of the clock genes, both at the level of their production and degradation, possibly by altering the usage of Aspartate codon.

Comments on revisions:

The authors addressed all my comments satisfactorily.

https://doi.org/10.7554/eLife.103427.3.sa2

Reviewer #3 (Public review):

Xiaoyu Wu and colleagues examined a potential role in sleep of a Drosophila ribosomal RNA methyltransferase, mettl5. Based on sleep defects reported in CRISPR generated mutants, the authors performed both RNA-seq and Ribo-seq analyses of head tissue from mutants and compared to control animals collected at the same time point. A major conclusion was that the mutant showed altered expression of circadian clock genes, and that the altered expression of the period gene in particular accounted for the sleep defect reported in the mettl5 mutant. In this revision, the authors have added a more thorough analysis of clock gene expression and show that PER protein levels are increased relative to wild type animals a specific times of day, indicating increased stability of the protein. Given that PER inhibits its own transcription, the per RNA is low in the mutants. The revised manuscript included efforts toward a more detailed understanding of how clock gene expression was altered in the mutants, as well as other clarification of sleep phenotypes.

Comments on revisions:

All critiques have been addressed by the authors; the manuscript is much improved from its original submission. Thank you.

https://doi.org/10.7554/eLife.103427.3.sa1

Author Response:

The following is the authors' response to the previous reviews

> ***Public Reviews:***
>
> ***Reviewer #1 (Public review):***
>
> *Here, the authors attempted to test whether the function of Mettl5 in sleep regulation was conserved in drosophila, and if so, by which molecular mechanisms. To do so they performed sleep analysis, as well as RNA-seq and ribo-seq in order to identify the downstream targets. They found that the loss of one copy of Mettl5 affects sleep, and that its catalytic activity is important for this function. Transcriptional and proteomic analyses show that multiple pathways were altered, including the clock signaling pathway and the proteasome. Based on these changes the authors propose that Mettl5 modulate sleep through regulation of the clock genes, both at the level of their production and degradation, possibly by altering the usage of Aspartate codon.*
>
> *Comments on revised version:*
>
> *The authors satisfactorily addressed my comments, even though the precise mechanism by which Mettl5 regulates translation of clock genes remains to be firmly demonstrated.*
>
> ***Reviewer #3 (Public review):***
>
> *Xiaoyu Wu and colleagues examined a potential role in sleep of a Drosophila ribosomal RNA methyltransferase, mettl5. Based on sleep defects reported in CRISPR generated mutants, the authors performed both RNA-seq and Ribo-seq analyses of head tissue from mutants and compared to control animals collected at the same time point. A major conclusion was that the mutant showed altered expression of circadian clock genes, and that the altered expression of the period gene in particular accounted for the sleep defect reported in the mettl5 mutant. In this revision, the authors have added a more thorough analysis of clock gene expression and show that PER protein levels are increased relative to wild type animals a specific times of day, indicating increased stability of the protein. Given that PER inhibits its own transcription, the per RNA is low in the mutants. Efforts toward a more detailed understanding of how clock gene expression was altered in the mutants, as well as other clarification of sleep phenotypes throughout is appreciated. As noted above, a strength of this work is its relevance to a human developmental disorder as well as the transcriptomic and ribosomal profiling of the mutant. However, there still remain some minor weaknesses in the manuscript. This reviewer is not in agreement with the interpretation of the epigenetic experiments. Specifically, co-expression of Clk[jrk] or per [01] with the mettl5 mutant recovered the nighttime sleep phenotype, but was additive to the daytime sleep phenotype such that double mutants showed higher sleep. This effect should be acknowledged and discussed. Overall, this is an interesting paper that indicates a molecular link between mettl5 and the circadian clock in regulation of sleep.*
>
> ***Recommendations for the authors:***
>
> ***Reviewer #3 (Recommendations for the authors):***
>
> *The authors misunderstood my original comment for Fig 1A. Please provide an explanation for the significance of the boxed region. There is little or no detail in the legend to help guide the reader.*

The information has been added to the figure legends for Figure 1A.

> *Efforts toward improving analysis of circadian genes as well as sleep phenotypes (sleep onset time, rebound, etc) is much appreciated, thank you. However, Figure S1H and G panel labels are mixed up; please label in the order that they appear and that they correspond to the main text. Why is Figure S1H labeled "ZT 14"?*

Sleep latency is defined as the time from preparing to sleep to actually falling asleep. In this study, it specifically refers to the time taken for each individual fly to reach the sleep phenotype (i.e., 25 minutes of continuous sleep). We noted that this label was misleading, as the actual time to reach the sleep phenotype varied among individual flies. Therefore, in the revised figures, we have removed the ZT14 label. In addition, we have corrected the labeling of Figures S1G and S1H to ensure they appear in the correct order and correspond accurately to the descriptions in the main text.

> *Unfortunately, based on Fig S1A-C, I am not convinced that mettl5 localizes to neurons, as there are no cells that show double labelling. This figure does not support the statement: "we found expression in both neurons (colocalizing with ELAV staining: Figure S1A-C) (lines 91-92), and "Mettl5-Gal4 is expressed in distinct neurons and glia that appear crucial for sleep regulation." (line 297). What "distinct" sleep related neurons were labeled? The staining in Fig S1A shows a different distribution from that in Fig S1D, and so it's possible this was a technical issue. Is there a better example?*

Thank you for your careful review and valuable comments. We agree that the colocalization of METTL5 with the neuronal marker ELAV is relatively sparse. However, as indicated by the arrows in Fig S1A–C, we did observe a few cells showing clear double labeling. These examples support the presence of METTL5 expression in neurons, albeit at a low frequency.

> *In Figure 4G-H, please indicate the time of day of tissue collection.*

In Figure 4G-H, the tissue was collected at ZT0. We have now indicated this time point in the figure and legend to clarify the experimental timing.

> *As noted in the public comment, I remain in disagreement with the assessment that "the double mutant showed the similar phenotype as downstream genes". The striking significant increase in daytime sleep in the double mutants remains unexplained. No further experiments are necessary, but this should be acknowledged in the text. Instead of an epistatic effect, given that overall sleep is high in the double mutants, another possible explanation is that the flies are sick and so are less active and sleeping more.*

Thank you for your suggestion. This has been acknowledged in the text. “Genetic epistasis experiments further supported this model, with clock gene mutants modified *Mettl5* mutant phenotypes that suggesting both Clock and Per downstream of *Mettl5* (Figure 4I-N, Table 1). Secondary effect may exist for the significant increase in daytime sleep in the double mutants.”

https://doi.org/10.7554/eLife.103427.3.sa0